Stability analysis of the flow in a cubical cavity heated from below

D. Puigjaner[(1)], C. Simó[(2)], F.X. Grau[(3)] and Francesc Giralt[(4)]

(1) Dept. Enginyeria Informàtica i Matemàtica, ETSE, Univ. Rovira i Virgili , Tarragona, Spain.

(2) Dept. Matemàtica Aplicada i Anàlisi, Fac. Matemàtiques, Univ. de Barcelona, Barcelona, Spain.

(3) Dept. Enginyeria Mecànica, ETSEQ, Univ. Rovira i Virgili, Tarragona, Spain.

(4) Dept. Enginyeria Química, ETSEQ, Univ. Rovira i Virgili, Tarragona, Spain.

Abstract

Bifurcations from the conductive state in a laterally insulated cubical cavity heated from below are examined. The perturbation equations for velocity and temperature are solved using a Galerkin method with a set of trial functions whose completeness within the cavity is proved. The set of trial functions satisfies boundary conditions and continuity so that pressure is eliminated and the stability problem reduces to an eigenvalue problem. Five different bifurcations from the conductive state, two at $Ra = 3389$ and one at $Ra = 5902$, 7458 and 8610, are identified together with the corresponding convective structures for Rayleigh numbers below 10^4. The stability of the five structures, one x–roll, a diagonal roll (x–roll $\pm$ y–roll), a four rolls structure (x–roll + y–roll with both rolls changing sense of rotation at the two central orthogonal vertical planes), a $2x$–rolls + $2y$–rolls and a $2x$–rolls − $2y$–rolls, is examined up to $Ra = 3 \times 10^4$. There is good agreement between the critical Rayleigh numbers and the velocity and temperature fields predicted by stability analysis and by previous numerical calculations. The effect of changing the aspect ratios on the critical Rayleigh numbers is also presented.

A non-linear stability analysis of the five convective structures identified shows that the single x–roll and the four rolls structures are stable, the former from the first birfucation from the conductive state and the latter beyond $Ra \approx 8900$. The diagonal single-roll structure is slightly unstable near the first bifurcation. Small numerical diffusion or experimental imperfections in previous numerical and experimental studies could cause the stabilization of this diagonal-roll. Both structures combining $2x$–rolls and $2y$–rolls are unstable. The non-linear analysis also shows that the $2x$–roll − $2y$–roll structure could bifurcate for $Ra > 3 \times 10^4$. Current results are in agreement with previous numerical and experimental studies reported in the literature.

1 Introduction

Natural convection arises when unstable density gradients occur in a fluid in the presence of an external field, usually a gravity field. In the Rayleigh-Bénard problem these gradients are produced by imposing an unstable vertical temperature difference in a laterally bounded or unbounded fluid layer. This flow system, which is governed by coupled non-linear equations for momentum and energy, provides an appropriate physical situation to study the onset of unsteadiness and transition from laminar to turbulent regimes (Busse, 1981; Yang, 1988). Reviews on Rayleigh-Bénard convection can be found in Normand et al. (1977), Busse (1978), Oertel (1982), Yang (1988), Koschmieder (1993) and Mukutmoni and Yang (1994).

The first bifurcation, which corresponds to the transition from the conductive state to the onset of convection, arises when the Rayleigh number or the dimensionless temperature difference between the bottom and the top plates, exceeds a given critical value. This transition is well documented in the literature for the unbounded case and for a variety of aspect ratios width/heigth and depth/heigth (h_1, h_2) of the enclosure (Davis, 1967; Catton, 1972; Heitz and Westwater, 1971; Stork and Muller, 1972, Arroyo and Savirón, 1991; Pallarès et. al, 1999a). These previous investigations reveal that the critical Rayleigh number decreases rapidly with an increase of the aspect ratio for aspect ratios h_2 less than 1 and approaches asymptotically the value of 1708, corresponding to transition in unbounded or infinite layers, when both aspect ratios are greater than 5. It has been also found that the convective structures developed at the onset of convection consist of a certain number of finite rolls with their axis of rotation parallel to the shorter side of the parallelepipedic cavity. These rolls have two non-zero velocity components which depend upon all three spatial variables.

The aim of this work is to apply a linear and a non-linear stability analysis to determine all the bifurcations and the stability of the flow structures that occur in the cubical cavity with adiabatic lateral walls heated from below for Rayleigh numbers up to 10^4. Numerical simulations of the same problem reported by Pallarès et al. (1999a) show that three critical Rayleigh numbers (3500, 6000 and 7800) exist for $Ra < 10^4$, giving rise to different stable or unstable flow structures. Only two of these structures could be confirmed following the linear stability analysis of Catton (1972) due to the incompleteness of the set of trial functions used in his work. In the present study the stability analysis of the Rayleigh-Bénard problem in a cubical cavity is performed using a complete set of trial functions. In addition to the cubical cavity problem, the effect of varying the aspect ratios h_1, h_2 on the onset of instability is also investigated.

The stability problem, presented in section 2 for both the linear and non-linear cases, is solved using the Galerkin procedure described in section 3. The completeness of the set of trial functions chosen to expand the velocity and the temperature functions within the cavity is proved in section 4. Since the trial functions satisfy all boundary conditions and continuity, pressure is eliminated and the linearized perturbation equations reduce to an eigenvalue problem, which is solved in section 5 using the power method. The non-linear stability study of the flow structures is performed in section 6. Finally, results for linear and non-linear studies are presented and discussed in section 7.

2 Physical model and governing equations

The physical model and the coordinate system are shown in Figure 1. The two horizontal plates are isothermal and the four vertical walls are considered perfectly insulated. The domain covered by the cubical cavity, scaled by the characteristic length L, is given by $\Omega = [-\frac{1}{2}, \frac{1}{2}] \times [-\frac{1}{2}, \frac{1}{2}] \times [-\frac{1}{2}, \frac{1}{2}]$.

In the following analysis ρ is the density of the fluid, g is the acceleration of gravity, θ_c and θ_h are the temperature at the top and the bottom of the cubical region, $\Delta\theta = \theta_h - \theta_c$, and β, ν and α are the coefficients of thermal expansion, kinematic viscosity and thermal diffusivity, respectively. All these physical properties are assumed to be constant. The Boussinesq approximation is used to determine the effect of density (ρ) in the buoyancy term.

The dimensionless coordinates are denoted as x, y and z. The characteristic scales for velocity $\vec{V} = (v^{(1)}, v^{(2)}, v^{(3)})$, temperature ($\theta$), time ($t$) and pressure ($p$) are $q_0 = [\beta(\Delta\theta)gL\alpha/\nu]^{\frac{1}{2}}$, $\Delta\theta$, L^2/α and $\rho\nu q_0/L$, respectively (Davis, 1967). The application of the Galerkin method to the governing linearized equations yields a linear algebraic system of equations whose matrix is symmetric when these scales are used.

The steady conductive state is described by a linear profile $\theta_s(z) = \theta_c + (z + 1/2)\Delta\theta$ and by $\vec{V} = 0$. Let $\theta(z)$ be the difference between the temperature and θ_s. The governing equations are

$$div\,\vec{V} = 0, \tag{1}$$

$$\frac{1}{Pr}\frac{\partial\vec{V}}{\partial t} - \nabla^2\vec{V} + \frac{Ra^{\frac{1}{2}}}{Pr}\sum_{i=1}^{3} v^{(i)} D_i\vec{V} - Ra^{\frac{1}{2}}\theta\,\vec{K} + \vec{\nabla}p = 0, \tag{2}$$

$$\frac{\partial\theta}{\partial t} - \nabla^2\theta + Ra^{\frac{1}{2}}\sum_{i=1}^{3} v^{(i)} D_i\theta - Ra^{\frac{1}{2}} v^{(3)} = 0 \tag{3}$$

with boundary conditions

$$\vec{V} = \theta = 0 \text{ on } |z| = \frac{1}{2}, \quad \vec{V} = \frac{\partial\theta}{\partial x} = 0 \text{ on } |x| = \frac{1}{2}, \quad \vec{V} = \frac{\partial\theta}{\partial y} = 0 \text{ on } |y| = \frac{1}{2}. \tag{4}$$

In equations (2) and (3) the Rayleigh number and the Prandtl number are defined as $Ra = \beta(\Delta\theta)gL^3/\alpha\nu$ and $Pr = \nu/\alpha$ respectively and $\vec{K}$ denotes the vector $(0, 0, 1)$.

The linearization of the steady state part of equations (1–3) yields,

$$div\,\vec{V} = 0, \tag{5}$$

$$\nabla^2\vec{V} + Ra^{\frac{1}{2}}\theta\,\vec{K} - \vec{\nabla}p = 0, \tag{6}$$

$$\nabla^2\theta + Ra^{\frac{1}{2}}\,v^{(3)} = 0 \tag{7}$$

with the same boundary conditions (4). From this set of equations it is clear that the onset of convection is independent of the Prandtl number.

These linearized equations do not include terms with time derivatives because Sherman and Ostrach (1966) proved that the principle of exchange of stabilities, i.e., transition to unstability occurs via a stationary state, is valid in this particular problem. This principle is characterized by the vanishing of both the real and the imaginary parts of the complex time eigenvalue associated with the disturbance. This is so because the real part of an eigenvalue must cross the zero value to have instability, and the eigenvalues are real because they appear as the eigenvalues of a selfadjoint operator (a symmetrical matrix in the discretizations). The systems (1–3) and (5–7), with boundary conditions (4), are not separable but approximate solutions may be obtained using the Galerkin procedure.

3 Galerkin procedure

Let us consider the sets

$$\Psi = \{\psi_n(x,y,z) \,|\, \psi_n = 0 \text{ on } |z| = \frac{1}{2},\ \frac{\partial \psi_n}{\partial x} = 0 \text{ on } |x| = \frac{1}{2},\ \frac{\partial \psi_n}{\partial y} = 0 \text{ on } |y| = \frac{1}{2}\} \tag{8}$$

and

$$\Phi = \{\vec{\phi}_n(x,y,z) \,|\, div\, \vec{\phi}_n = 0,\ \vec{\phi}_n = 0 \text{ on } \partial\Omega\}. \tag{9}$$

The variables $\vec{V}$, θ and p are expanded according to

$$\vec{V} = \sum_{n=1}^{\infty} c_n \vec{\phi}_n\,, \quad \theta = \sum_{n=1}^{\infty} d_n \psi_n\,, \quad p = \sum_{n=1}^{\infty} e_n \xi_n\,, \tag{10}$$

where there is no need to specify the base functions ξ_n for the pressure since it will be eliminated. Expansions (10) are truncated to

$$\vec{V} = \sum_{n=1}^{N} c_n \vec{\phi}_n\,, \quad \theta = \sum_{n=1}^{M} d_n \psi_n\,, \quad p = \sum_{n=1}^{L} e_n \xi_n \tag{11}$$

and substituted into the governing equations (2–3) or the linearized ones (6–7). The continuity equation (1) or (5) and boundary conditions (4) are satisfied because of the choice of the sets Ψ and Φ defined in (8) and (9), respectively. Since the solution of equations (2–3) or (6–7) written in terms of the basis functions will not be exact because the truncated expansions (11) are used, a Galerkin method is applied to find approximate solutions. The Galerkin method imposes the error to be orthogonal to any vector of the form,

$$\begin{pmatrix} \vec{\phi}_j \\ \psi_k \end{pmatrix} = \begin{pmatrix} \phi_j^{(1)} \\ \phi_j^{(2)} \\ \phi_j^{(3)} \\ \psi_k \end{pmatrix}, \quad j = 1,\ldots,N\,, \quad k = 1,\ldots,M\,. \tag{12}$$

In order to obtain good approximations it must be ensured that the functions (10) chosen to expand the velocity and the temperature form a complete set of functions within the cavity.

4 Trial functions

Let us consider:

$$\theta \in T = \{\Psi \cap L^2(\Omega)\}; \qquad \vec{V} \in E = \{\vec{\phi} \in \Phi \mid D_i \phi^{(k)} \in L^1(\Omega)\} \tag{13}$$

The objective of the present section is to prove that complete sets of trial functions on the spaces T and E can be built. The method used here to select trial functions is that of Catton (1972), but several sets of functions have been added to the original Catton's set to ensure its completeness.

Let $\Omega = I_1 \times I_2 \times I_3$ with I_1, I_2, I_3 closed intervals in $\mathbb{R}$. Let us assume that the sets $\{f_i\}$, $\{g_j\}$ and $\{h_k\}$ constitute an orthogonal basis on $L^2(I_1)$, $L^2(I_2)$ and $L^2(I_3)$, respectively, so that the set $\{F_{ijk}(x,y,z) = f_i(x) g_j(y) h_k(z)\}$ is an orthogonal basis on $L^2(\Omega)$. This is important to construct a complete set of trial functions.

Since it is known that the eigenfunctions of a Sturm-Liouville problem on an interval G form an orthogonal complete basis for $L^2(G)$ whose elements satisfy boundary conditions (Canuto, 1987; Showalter, 1979) the following Sturm-Liouville problems on $I = [-\frac{1}{2}, \frac{1}{2}]$ will be considered:

$$\left\{ \begin{array}{l} f'' = af \\ f(-1/2) = f(1/2) = 0 \end{array} \right\} \quad ; \quad \left\{ \begin{array}{l} f'' = af \\ f'(-1/2) = f'(1/2) = 0 \end{array} \right\}$$

and

$$\left\{ \begin{array}{l} f^{(IV)} = af \\ f(-1/2) = f(1/2) = 0 \\ f'(-1/2) = f'(1/2) = 0 \end{array} \right\},$$

whose respective eigenfunctions are:

$$g_k(x) = \left\{ \begin{array}{l} \cos((2k-1)\pi x) \\ \text{or} \\ \sin(2k\pi x) \end{array} \right. \tag{14}$$

$$h_k(x) = \left\{ \begin{array}{l} \cos(2(k-1)\pi x) \\ \text{or} \\ \sin((2k-1)\pi x) \end{array} \right. \tag{15}$$

$$f_k(x) = \left\{ \begin{array}{l} C_k(x) = \dfrac{\cosh(\lambda_k x)}{\cosh(\lambda_k/2)} - \dfrac{\cos(\lambda_k x)}{\cos(\lambda_k/2)} \\ \text{or} \\ S_k(x) = \dfrac{\sinh(\mu_k x)}{\sinh(\mu_k/2)} - \dfrac{\sin(\mu_k x)}{\sin(\mu_k/2)} \end{array} \right. \tag{16}$$

The parameters λ_k and μ_k in (16) are the positive roots of equations $\tanh(\lambda_k/2) + \tan(\lambda_k/2) = 0$ and $\tanh(\mu_k/2) - \tan(\mu_k/2) = 0$, respectively. If $0 < \lambda_1 < \lambda_2 < \cdots$, and $0 < \mu_1 < \mu_2 < \cdots$, then $\lambda_k \simeq 2k\pi - \dfrac{\pi}{2}$ and $\mu_k \simeq 2k\pi + \dfrac{\pi}{2}$, for large k. The functions C_k and S_k are even and odd functions with a cosine and sine-like behaviour, respectively. The even function C_k vanishes $2k$ times along the interval $[-\frac{1}{2}, \frac{1}{2}]$, while the odd function S_k has $2k+1$ roots in the same interval. This general behavior is shown in Figure 2 for the first two C_k and S_k. Several integrals involving these functions and their derivatives are found in Harris and Reid (1959).

Since $\Omega = I \times I \times I$, the set

$$\{\phi_{ijk}(x,y,z) = h_i(x)h_j(y)g_k(z)\}_{ijk}\,, \tag{17}$$

with g and h defined by expressions (14–15), forms an orthogonal complete basis on T. The basis given in (17) is used to expand θ.

In order to construct a basis for E it is splitted according to

$$\begin{aligned} E &= E_1 \oplus E_2 \\ E_1 &= \{(v^{(1)}, 0, v_1^{(3)})^T \in E \;\mid\; \partial v^{(1)}/\partial x = -\partial v_1^{(3)}/\partial z\}\,, \\ E_2 &= \{(0, v^{(2)}, v_2^{(3)})^T \in E \;\mid\; \partial v^{(2)}/\partial y = -\partial v_2^{(3)}/\partial z\}\,, \end{aligned} \tag{18}$$

so that any general solution can be obtained as a sum of two kinds of finite rolls, the x–rolls (zero y component of velocity) and the y–rolls (zero x component of velocity).

The use of the equivalences

$$
\begin{aligned}
&(v^{(1)},0,v_1^{(3)})^T \in E_1 \Longleftrightarrow \exists\, \varphi(x,y,z) \in L^2(\Omega) \text{ verifying } v^{(1)} = -\frac{\partial \varphi}{\partial z},\; v_1^{(3)} = \frac{\partial \varphi}{\partial x}\,, \\
&(0,v^{(2)},v_2^{(3)})^T \in E_2 \Longleftrightarrow \exists\, \tau(x,y,z) \in L^2(\Omega) \text{ verifying } v^{(2)} = -\frac{\partial \tau}{\partial z},\; v_2^{(3)} = \frac{\partial \tau}{\partial y}\,,
\end{aligned}
\tag{19}
$$

is sufficient to provide suitable bases to expand φ and τ,

$$
\begin{aligned}
&\{\varphi_{i,j,k}(x,y,z) = f_i(x) g_j(y) f_k(z)\}\,, \\
&\{\tau_{i,j,k}(x,y,z) = g_i(x) f_j(y) f_k(z)\}\,.
\end{aligned}
\tag{20}
$$

Therefore the sets

$$
\{\vec{\eta}(x,y,z)\}_{ijk} = \left\{ \begin{pmatrix} f_i(x) g_j(y) f_k'(z) \\ 0 \\ -f_i'(x) g_j(y) f_k(z) \end{pmatrix} \right\}_{ijk} \tag{21}
$$

and

$$
\{\vec{\vartheta}(x,y,z)\}_{ijk} = \left\{ \begin{pmatrix} 0 \\ g_i(x) f_j(y) f_k'(z) \\ -g_i(x) f_j'(y) f_k(z) \end{pmatrix} \right\}_{ijk} \tag{22}
$$

with g, h and f defined by (14–16), form complete bases of E_1 and E_2, respectively. In (21–22) the prime denotes differentiation with respect to the current argument.

5 Linear stability analysis

Let us consider $\{\vec{F}_l\}$ a complete set of trial functions on the spaces T and E. Any solution of the linearized equations (5–7) is expanded and truncated according to

$$
\vec{a}(x,y,z) = \begin{pmatrix} \vec{V}(x,y,z) \\ \theta(x,y,z) \end{pmatrix} = \sum_{l=1}^{\infty} a(l) \vec{F}_l(x,y,z)\,. \tag{23}
$$

As a result of applying the Galerkin procedure, described in section 3, to the linearized equations (6–7), the following linear algebraic equations are obtained

$$
\sum_{i=1}^{L} (l_1(i,j) + Ra^{\frac{1}{2}} l_2(i,j)) a(i) = 0\,, \tag{24}
$$

where

$$
l_1(i,j) = \left\langle \begin{pmatrix} \nabla^2 F_i^{(1)} \\ \nabla^2 F_i^{(2)} \\ \nabla^2 F_i^{(3)} \\ \nabla^2 F_i^{(4)} \end{pmatrix}, \begin{pmatrix} F_j^{(1)} \\ F_j^{(2)} \\ F_j^{(3)} \\ F_j^{(4)} \end{pmatrix} \right\rangle \quad , \quad l_2(i,j) = \left\langle \begin{pmatrix} 0 \\ 0 \\ F_i^{(3)} \\ F_i^{(4)} \end{pmatrix}, \begin{pmatrix} F_j^{(1)} \\ F_j^{(2)} \\ F_j^{(3)} \\ F_j^{(4)} \end{pmatrix} \right\rangle \tag{25}
$$

The use of the basis (17) for the temperature function and (21–22) for the velocity function, as well as a suitable ordering of the elements of the basis and of the equations, yields the linear system

$$
M(Ra) \begin{pmatrix} a_1 \\ \vdots \\ a_L \end{pmatrix} = \vec{0}\,, \tag{26}
$$

whose matrix M is block-diagonal with eigth different blocks ($M_i,\ i = 1, \ldots, 8$).

The associated trial functions $\{\vec{F}_m\}_{m=1,\ldots,3N}$ within any block have the form

$$\vec{F}_m = \begin{pmatrix} \vec{\eta}_{ijk} \\ 0 \end{pmatrix} \quad , \quad \vec{F}_{N+m} = \begin{pmatrix} \vec{\vartheta}_{ijk} \\ 0 \end{pmatrix} \quad , \quad \vec{F}_{2N+m} = \begin{pmatrix} \vec{0} \\ \phi_{ijk} \end{pmatrix} \tag{27}$$

for $i = 1, \ldots, n_x,\ j = 1, \ldots, n_y$ and $k = 1, \ldots, n_z$. The indexes n_x, n_y and n_z are the number of trial functions used in the x, y and z direction, respectively. $N = n_x \times n_y \times n_z$, $m = (i-1)\, n_y \times n_z + (j-1)\, n_z + k$ and $\vec{\eta}_{ijk}$, $\vec{\vartheta}_{ijk}$ and ϕ_{ijk} are defined in expressions (21), (22) and (17), respectively.

Each one of these blocks M_l has the structure

$$M_l(Ra) = \begin{vmatrix} A_l & Ra^{\frac{1}{2}} B_l^T \\ Ra^{\frac{1}{2}} B_l & C_l \end{vmatrix} . \tag{28}$$

In this expression A_l, B_l, C_l are $2N \times 2N$, $N \times 2N$ and $N \times N$ matrices, respectively, defined as

$$A_l(i,j) = \langle \nabla^2 \vec{F}_i,\, \vec{F}_j \rangle; \quad B_l(i,j) = \langle F_i^{(4)},\, F_j^{(3)} \rangle\,; \quad C_l(i,j) = \langle \nabla^2 F_i^{(4)},\, F_j^{(4)} \rangle\,. \tag{29}$$

Each block corresponds to one of the two possible choices in expressions (14–16). The blocks have been numbered so that the functions chosen in expressions (14–16) for any block M_l, $l = 1, \ldots, 8$, are either the functions

$$\begin{array}{l} \left\{ \begin{array}{l} h_i(x) = \sin((2i-1)\pi x) \\ f_i(x) = C_i(x) \\ g_i(x) = \sin(2i\pi x) \end{array} \right\} \Longleftrightarrow \left\{ \begin{array}{ll} l \equiv 1 & (4) \\ \text{or} & \\ l \equiv 2 & (4) \end{array} \right\}; \\ \left\{ \begin{array}{l} h_j(y) = \cos(2(j-1)\pi y) \\ g_j(y) = \cos((2j-1)\pi y) \\ f_j(y) = S_j(y) \end{array} \right\} \Longleftrightarrow \left\{ \begin{array}{ll} l \equiv 1 & (4) \\ \text{or} & \\ l \equiv 3 & (4) \end{array} \right\}; \\ \left\{ \begin{array}{l} g_k(z) = \cos((2k-1)\pi z) \\ f_k(z) = C_k(z) \end{array} \right\} \Longleftrightarrow l \in \{1,2,3,4\} \end{array} \tag{30}$$

or the alternative functions for the other l values.

The kind of functions of each block determines which type of x–rolls and y–rolls are involved. According to the coordinate system of Figure 1 with $\xi = x$ or y, the following correspondences can be established:

$$\begin{array}{l} f_m(\xi) = C_m(\xi) \leftrightarrow (2m-1)\ \xi\text{–roll}, \\ f_m(\xi) = S_m(\xi) \leftrightarrow (2m)\ \xi\text{–roll}, \\ f_k(z) = C_k(z) \leftrightarrow \text{ changes } 2(k-1) \text{ times the sense of } z\text{–rotation}, \\ f_k(z) = S_k(z) \leftrightarrow \text{ changes } (2k-1) \text{ times the sense of } z\text{–rotation}, \\ g_m(\xi) = \cos((2m-1)\pi\xi) \leftrightarrow \text{ changes } 2(m-1) \text{ times the sense of } \xi\text{–rotation}, \\ g_m(\xi) = \sin(2m\pi\xi) \leftrightarrow \text{ changes } (2m-1) \text{ times the sense of } \xi\text{–rotation}, \end{array} \tag{31}$$

Thus, the number of a trial function and that of the block, together with expressions (27), (30) and (31), are sufficient to determine which kind of roll develops. Several examples of these rolls are given in Table I for the case $n_x = n_y = n_z = 5$.

Therefore, equation (24) has a non trivial solution if and only if

$$\exists l \in \{1, \ldots, 8\} \ \mid \ det\, M_l(Ra) = 0, \tag{32}$$

which is equivalent to finding a non trivial solution $(a_1, \ldots, a_{3N})^T$ in

$$\left(A_l^{-1} B_l^T C_l^{-1} B_l - \frac{1}{Ra}\right) \begin{pmatrix} a_1 \\ \vdots \\ a_{2N} \end{pmatrix} = 0, \tag{33}$$

$$\begin{pmatrix} a_{2N+1} \\ \vdots \\ a_{3N} \end{pmatrix} = -Ra^{\frac{1}{2}} C_l^{-1} B_l \begin{pmatrix} a_1 \\ \vdots \\ a_{2N} \end{pmatrix}. \tag{34}$$

Therefore the linear stability problem reduces to an $2N \times 2N$ eigenvalue problem for the Rayleigh number. The critical Rayleigh number Ra_c, i.e., the smallest positive value of Ra for which there exists l with $\det M_l(Ra) = 0$, is then the inverse of the greatest positive eigenvalue of $(A_l^{-1} B_l^T C_l^{-1} B_l)$.

Equations (33–34) were solved for the eight eigenvalue problems using the power method, refined with a shift and the inverse power method, and increasing the number of trial functions until the difference of the estimates of the largest eigenvalue was smaller than 10^{-4}. For a relatively small number of trial functions, i.e., for $\dim(M_i)$ less than 500, all eigenvalues can be determined following any standard procedure.

It should be noted that if $n_x = n_y = n_z$ is increased from 3 to 5 and the eigenvalues are ordered by decreasing real part, the first additional eigenvalue appears, in the worse case, in the position 12. When $n_x = n_y = n_z$ is increased from 5 to 7, this happens in the position 59. For these computations we have considered values of Ra up to 3×10^4, as through all the paper.

6 Non-linear stability analysis

6.1 Equations

Linear stability analysis cannot determine which kind of flow will occur when the critical Ra is a multiple eigenvalue, such as it happens when two bifurcation curves intersect, because any linear combination of the independent eigenvectors is possible. In this situation a non-linear analysis is necessary in order to know which combinations take place. This latter situation happens whenever the minimum critical Rayleigh number curve presents a kink. Precisely, fixing $h_1 = 1$, the first kink on the curve corresponds to the cubical case. A non-linear analysis is also needed to determine whether the structures which appear at critical Rayleigh numbers, beyond the first one, and that are unstable according to the linear theory, become stable, because of a new bifurcation, at certain distance of the critical ones. This non-linear analysis is the objective of this section.

Expanding and truncating any solution of the nonlinear equations (1–3) according to

$$\vec{a}(t, x, y, z) = \sum_{l=1}^{L} a(l) \vec{F}_l(x, y, z), \tag{35}$$

where $a(l)$ denotes a function depending on t, and applying the Galerkin procedure, the following system of ordinary differential equations is obtained:

$$\sum_{i=1}^{L} b(i,j) a'(i) = \sum_{i=1}^{L} (l_1(i,j) + Ra^{\frac{1}{2}} l_2(i,j)) a(i) - \frac{Ra^{\frac{1}{2}}}{2} \sum_{i=1}^{L} \sum_{n=1}^{L} q(i,n,j) a(i) a(n), \quad j = 1, \ldots, L, \tag{36}$$

where

$$b(i,j) = \langle \begin{pmatrix} \frac{1}{Pr}F_i^{(1)} \\ \frac{1}{Pr}F_i^{(2)} \\ \frac{1}{Pr}F_i^{(3)} \\ F_i^{(4)} \end{pmatrix}, \begin{pmatrix} F_j^{(1)} \\ F_j^{(2)} \\ F_j^{(3)} \\ F_j^{(4)} \end{pmatrix} \rangle \,, \tag{37}$$

$$q(i,n,j) = \langle \begin{pmatrix} \frac{1}{Pr}\sum_{r=1}^{3} F_i^{(r)} D_r F_n^{(1)} \\ \frac{1}{Pr}\sum_{r=1}^{3} F_i^{(r)} D_r F_n^{(2)} \\ \frac{1}{Pr}\sum_{r=1}^{3} F_i^{(r)} D_r F_n^{(3)} \\ \sum_{r=1}^{3} F_i^{(r)} D_r F_n^{(4)} \end{pmatrix}, \begin{pmatrix} F_j^{(1)} \\ F_j^{(2)} \\ F_j^{(3)} \\ F_j^{(4)} \end{pmatrix} \rangle + \langle \begin{pmatrix} \frac{1}{Pr}\sum_{r=1}^{3} F_j^{(r)} D_r F_n^{(1)} \\ \frac{1}{Pr}\sum_{r=1}^{3} F_j^{(r)} D_r F_n^{(2)} \\ \frac{1}{Pr}\sum_{r=1}^{3} F_j^{(r)} D_r F_n^{(3)} \\ \sum_{r=1}^{3} F_j^{(r)} D_r F_n^{(4)} \end{pmatrix}, \begin{pmatrix} F_i^{(1)} \\ F_i^{(2)} \\ F_i^{(3)} \\ F_i^{(4)} \end{pmatrix} \rangle \tag{38}$$

and $l_1(i,j)$, $l_2(i,j)$ are defined in expression (25).

In equation (36) the prime means differentiation with respect to the time. If $nb(i)$ denotes the block associated to the trial function F_i, it is elementary to verify the following facts about the coefficients of equation (36)

$$\begin{array}{rcl} \left\{ \begin{array}{l} l_1(i,j) \neq 0 \\ l_2(i,j) \neq 0 \end{array} \right\} & \Longleftrightarrow & nb(i) = nb(j)\,, \\ q(i,n,j) \neq 0 & \Longleftrightarrow & (nb(i), nb(n), nb(j)) \in \mathcal{S}\,, \end{array} \tag{39}$$

where

$$\begin{array}{rcl} \mathcal{S} & = & \{\wp(1,2,8),\ \wp(1,3,5),\ \wp(1,4,6),\ \wp(2,3,6),\ \wp(2,4,5),\ \wp(3,4,8),\ \wp(5,6,8)\} \\ & & \cup(\cup_{j=1,\ldots,8}\{\wp(j,j,7)\}) \end{array}$$

and $\wp(i,j,k)$ denotes the group of permutations of three elements.

In order to achieve the objective of this section the following steps are carried out:

1. Find stationary solutions of the nonlinear equation (36) for a value of Ra near a critical one.

2. Apply a continuation method to calculate stationary solutions of the nonlinear equation (36) for different values of Ra.

3. Determine the stability of previously calculated stationary solutions.

6.2 Stationary solutions near a critical Rayleigh

Let us consider a Rayleigh number Ra_0 near a critical Rayleigh Ra_c and $\{\vec{\varphi}_k\}_k$ an orthogonal basis whose elements are the eigenvectors of the matrix $M(Ra_0)$ associated to the linearized equations (24). Any stationary solution of equation (36) is expanded and truncated to

$$\vec{a} = \sum_{l=1}^{L} a(l)\vec{\varphi}_l \tag{40}$$

The substitution of equation (40) into equation (36) yields

$$\vec{g}(a(1),\ldots,a(L)) = \begin{pmatrix} -\lambda_1 a(1) + \frac{Ra_0^{\frac{1}{2}}}{2}\sum_{i=1}^{L}\sum_{n=1}^{L} q(i,n,1)a(i)a(n) \\ \vdots \\ -\lambda_L a(L) + \frac{Ra_0^{\frac{1}{2}}}{2}\sum_{i=1}^{L}\sum_{n=1}^{L} q(i,n,L)a(i)a(n) \end{pmatrix} = \vec{0}, \qquad (41)$$

where λ_j is the eigenvalue corresponding to the basis function $\vec{\varphi}_j$. A solution of equation (41) can be estimated using the Newton method, but an approximate trial solution is necessary to start the procedure. To this end we proceed to a standard bifurcation analysis (Simó, 1990).

Let us denote λ_k and $\vec{\varphi}_k$ respectively the eigenvalue and the eigenvector associated to the critical Rayleigh Ra_c. Since Ra_0 is close to Ra_c it can be assumed that λ_k is nearly 0. Guided by the generic behavior at a pitchfork bifurcation, the coefficients $a(l)$ in equation (41) are scaled to

$$\begin{cases} \hat{a}(k) = a(k)/\lambda_k^{\frac{1}{2}}\,, \\ \hat{a}(l) = a(l)/\lambda_k \qquad \text{if} \quad l \neq k \end{cases} \qquad (42)$$

and then λ_k is substituted by zero. The following equations are obtained

$$\begin{cases} \hat{a}(k) - Ra_0^{\frac{1}{2}} \sum_{nb(l)=7} q(l,k,k)\hat{a}(l)\hat{a}(k) = 0\,, & \\ \lambda_l \hat{a}(l) - \frac{Ra_0^{\frac{1}{2}}}{2} q(k,k,l)\hat{a}(k)^2 = 0 & \text{if} \quad nb(l) = 7\,, \\ \hat{a}(l) = 0 & \text{if} \quad nb(l) \neq 7, \quad l \neq k\,. \end{cases} \qquad (43)$$

Solutions of equation (43) are the initial guesses to solve (41) by means of the Newton method.

For the cubical cavity, blocks M_1 and M_5 have the same eigenvalues as blocks M_4 and M_8, respectively. This fact means that any eigenvalue λ_k associated to these blocks is a double eigenvalue with two linearly independent eigenvectors $\vec{\varphi}_k$ and $\vec{\varphi}_j$. In this case equation (43) becomes

$$\begin{cases} \hat{a}(k) - Ra_0^{\frac{1}{2}}\Big(\sum_{nb(l)=7} q(l,k,k)\hat{a}(l)\hat{a}(k) + \sum_{nb(l)=6} q(l,j,k)\hat{a}(l)\hat{a}(j)\Big) = 0\,, & \\ \hat{a}(j) - Ra_0^{\frac{1}{2}}\Big(\sum_{nb(l)=7} q(l,j,j)\hat{a}(l)\hat{a}(j) + \sum_{nb(l)=6} q(l,k,j)\hat{a}(l)\hat{a}(k)\Big) = 0\,, & \\ \lambda_l \hat{a}(l) - \frac{Ra_0^{\frac{1}{2}}}{2}\big(q(k,k,l)\hat{a}(k)^2 + q(j,j,l)\hat{a}(j)^2\big) = 0 & \text{if} \quad nb(l) = 7\,, \\ \lambda_l \hat{a}(l) - Ra_0^{\frac{1}{2}} q(k,j,l)\hat{a}(k)\hat{a}(j) = 0 & \text{if} \quad nb(l) = 6\,, \\ \hat{a}(l) = 0 & \text{if} \quad nb(l) \neq 6,\ 7,\ l \neq k,\ j\,. \end{cases} \qquad (44)$$

Equation (43) yields initial solutions that belong to the space generated by the basis functions associated to blocks $M_{nb(k)}$ and M_7, while equation (44) yields solutions associated to blocks $M_{nb(k)}$, $M_{nb(j)}$, M_7 and M_6. It can be proved that when the Newton method is applied these restrictions are kept. Therefore, any solution of equation (41) belongs either to the subspace generated by the basis functions associated to a pair of blocks (M_7, and any other) or to the subspace generated by the the basis functions associated to four blocks (M_6, M_7, and M_1, M_4 or M_5, M_8).

6.3 Continuation method

Using the Galerkin method with the truncated expansions (40) the problem to find stationary solutions of equation (36) reduces to the following nonlinear system of equations

$$\vec{g}\begin{pmatrix} a(1) \\ \vdots \\ a(L) \\ a(L+1) \end{pmatrix} = \begin{pmatrix} -\sum_{i=1}^{L}(l_1(i,1)+10^2 a(L+1)^{\frac{1}{2}} l_2(i,1))a(i)+ \\ +\frac{10^2 a(L+1)^{\frac{1}{2}}}{2}\sum_{i=1}^{L}\sum_{n=1}^{L} q(i,n,1)a(i)a(n) \\ \vdots \\ -\sum_{i=1}^{L}(l_1(i,L)+10^2 a(L+1)^{\frac{1}{2}} l_2(i,L))a(i)+ \\ +\frac{10^2 a(L+1)^{\frac{1}{2}}}{2}\sum_{i=1}^{L}\sum_{n=1}^{L} q(i,n,L)a(i)a(n) \end{pmatrix} = \vec{0}, \qquad (45)$$

where $a(L+1) = 10^{-4} Ra$.

The continuation method consists in the use of a modified Newton method (Simó, 1990) to find a solution $\vec{a}_n^T = (a_n(1), \ldots, a_n(L), a_n(L+1))^T$ of equation (45) near a known solution $\vec{a}_0^T = (a_0(1), \ldots, a_0(L), a_0(L+1))^T$. A solution near a critical Rayleigh obtained following the method described in section 6.2 is taken as the initial known solution. Each one of these initial solutions belongs to a certain subspace (see the last paragraph in the previous section). It should be noted that solutions do not leave the subspace when applying the modifided Newton procedure. As a consequence any stationary solution of equation (45) is constrained to a subspace of the space generated by the trial functions.

The iterative modified Newton procedure performed here has the form

$$\vec{a}_n^{(k+1)} = \vec{a}_n^{(k)} - (Dg(\vec{a}_n^{(k)}))^T \left[Dg(\vec{a}_n^{(k)})(Dg(\vec{a}_n^{(k)}))^T\right]^{-1} g(\vec{a}_n^{(k)}), \qquad (46)$$

where $Dg(\vec{a})$ denotes the $L \times (L+1)$ Jacobian matrix. The following initial trial solution is used to start the Newton procedure:

$$\begin{cases} \vec{a}_n^{(0)} = \vec{a}_o + \Delta s\, \vec{v}\,, \\ \vec{v} \in ker\, Dg(\vec{a}_0)\,. \end{cases} \qquad (47)$$

6.4 Stability analysis

The linearization of equation (36) around a stationary solution $\vec{a}^e = (a^e(1), \ldots, a^e(L)) = \sum_{l=1}^{L} a^e(l)\vec{\varphi}_l$ yields the variational equation

$$\frac{d\alpha}{dt} = (B^{-1}\, Dg(\vec{a}^e))\,\alpha\,. \qquad (48)$$

In this equation B and $Dg(\vec{a}^e))$ are the $L \times L$ matrices defined as

$$\begin{aligned} B(i,j) &= -b(i,j) \\ Dg(i,j) &= -l_1(j,i) + Ra^{\frac{1}{2}}\left(-l_2(j,i) + \sum_{l=1}^{L} q(j,l,i)a^e(l)\right), \end{aligned} \qquad (49)$$

with b, l_1 and l_2, and q defined respectively by expressions (37), (25) and (38).

Therefore the non-linear stability problem reduces again to an eigenvalue problem but in this case for the matrix $B^{-1}\,Dg(\vec{a}^e)$. A solution $\vec{a}^e$ is stable if and only if all the eigenvalues of $B^{-1}\,Dg(\vec{a}^e)$ have negative real part. It should be noted that the flow structures developed at the critical Rayleigh numbers beyond the first one, are unstable according to linear theory. However they can become stable for values of Ra strictly greater than the critical ones.

7 Results and discussion

7.1 The cubical cavity

The linear stability analysis in the cubical Rayleigh-Bénard problem performed by Catton (1972) showed that the smallest critical Rayleigh number is 3446. At this critical value a single x or y–roll structure develops. On the other hand, the direct numerical simulations of this flow carried out by Hernández and Frederick (1994) and by Pallarès et al. (1999a) have revealed that two additional critical Rayleigh numbers appear below $Ra = 10^4$. The present work proves, using the complete set of trial functions given in section 4, that four critical Rayleigh numbers exist for values of $Ra < 10^4$. These critical values and the corresponding type of flow structure developed are summarized in Table II together with the values reported by Catton (1972), Hernández and Frederick (1994) and by Pallarès et al. (1999a) . There is good agreement between the present analysis of the bifurcations from the conductive state in a cubical cavity and the critical Rayleigh numbers reported in the literature.

According to linear theory the Rayleigh number becomes a bifurcation point or a critical value Ra_c when M_i has a zero eigenvalue for some $i \in \{1, \ldots, 8\}$. Whenever the eigenvalue is simple the associated normalized eigenvector describes, qualitatively, the type of flow developed at the bifurcation point. That is, the solution is close to a multiple of that eigenvector. However a non-linear study is necessary to determine the norm of the approximate solution near the critical Rayleigh and to know the evolution of the flow structure beyond this value. The variation of several of the largest eigenvalues computed from the linearized equations for the eight blocks with Ra is given in Figure 3. This figure displays the four critical Rayleigh numbers or zero crossings obtained for values of $Ra < 10^4$ and also shows that blocks M_5, M_6, M_7 and M_8 become positive only for $Ra > 2 \times 10^4$. For the cubical cavity blocks M_1 and M_5 are equivalent to blocks M_4 and M_8, respectively, when x and y are exchanged and, therefore, their eigenvalues become multiple eigenvalues.

The present study predicts that the smallest critical Rayleigh number is 3389. This critical Rayleigh number is an eigenvalue for both M_1 and M_4, indicating that any linear combination of the two eigenfunctions, i.e., of one x–roll and one y–roll, is possible according to linear stability analysis. Nevertheless, only two of these structures, a single x or y–roll and a diagonal-roll, are found when applying nonlinear theory, in agreement with the structures found numerically by Pallarès et al. (1999a). The first structure, named $S1$ following the notation of these authors, is formed by one x–roll (or, by exchanging the roles of x and y, by one y–roll) while the second one, named $S2$, is also a single roll but with a diagonal mode of circulation. This mode is obtained, in the linear approximation, by substracting one x–roll from one y–roll. In a similar way, a symmetric solution is found by adding them. At the second critical Rayleigh number of 5902 a four rolls flow structure, named $S5$, is developed. It is associated with the block M_2 and is the

sum of one x–roll and one y–roll, each roll changing sense of rotation at the two central orthogonal vertical planes of the cavity. This Ra_c value of 5902 can not be predicted by the incomplete set of functions proposed by Catton (1972). Structure $S4$ which develops at the third critical Rayleigh number of 7458 is associated to the block M_3 and has a toroidal configuration. The present analysis shows that $S4$ is the sum of two x–rolls and two y–rolls with no change of rotation along their axes. Finally a fifth structure $S6$, also associated with the block M_3, is predicted by the stability analysis at $Ra \approx 8610$. This structure, which corresponds to the substraction of two x–rolls and two y–rolls, has not been found by finite difference calculations near its critical Rayleigh.

As it was mentioned in 6.4 a solution $\vec{a}^e$ is stable if and only if all the eigenvalues of $B^{-1}\, Dg(\vec{a}^e))$ have negative real part. The variation of the main eigenvalue of this matrix is depicted in Figure 4 as a function of Ra for the different flow structures ($S1$, $S2$, $S4$, $S5$ and $S6$) obtained in the current work. This figure shows that structures $S2$, $S4$, and $S6$ are unstable for values of Ra up to 2×10^4. Structure $S2$ is the less unstable of the three because its only positive eigenvalue remains close to zero in Figure 4 near the Ra_c. Structure $S4$ has two additional positive eigenvalues beyond the principal one plotted in Figure 4. These three positive eigenvalues increase with Ra, explaining the highly unstable character of $S4$. Three of the four positive eigenvalues of structure $S6$, not depicted in Figure 4, decrease with Rayleigh number, with one of them approaching zero at $Ra = 3 \times 10^4$. This suggests that $S6$ may bifurcate and stabilize into a similar or different motion beyond 3×10^4. The experimental results of Pallarès et al. (1999b) provide evidence of this possibility.

The present stability analysis shows that only structures $S1$ and $S5$ are stable within the range of Rayleigh numbers covered. Structure $S5$ is unstable when it appears, as shown by the positive double eigenvalue given in Figure 4. This double eigenvalue becomes negative at $Ra \approx 8900$ and, thus, $S5$ becomes stable and remains so thereafter. The current study has not examined whether other structures appear at the bifurcation $Ra \approx 8900$ in addition to $S5$. The single roll $S1$ is stable over the whole range of Ra considered.

Pallarès et al. (1999b) reported that the only structures that can be found experimentally are the stable structures $S1$ and $S5$ and the slightly unstable structure $S2$. The fact that this unstable structure $S2$ is found experimentally may be due to the impossibility of implementing experimentally a perfect cubical geometry with perfect adiabatic lateral walls, particularly at the four vertical edges. The same applies to the stabilization effects caused by numerical diffusion in the numerical calculations of Pallarès et al. (1999a). When this diffusion is reduced and the numerical calculations are carried out over a sufficient period of time for the perturbations to grow, this diagonal-roll evolves into the stable $S1$–roll, as mentioned by Pallarès et al. (1999b). These authors also reported that structure $S4$ just appears experimentally as a transitory structure towards $S1$ when convection begins inside the cavity. Furthermore, the effects of perturbations caused by slightly changing the aspect ratio or tilting the cavity reported in Pallarès et al. (1999a) confirm the unstable character of $S2$, $S4$ and $S6$. Therefore, there is good agreement between the present study and previous experimental and numerical results.

Figures 5 to 9 depict the velocity and temperature fields of structures $S1$, $S2$, $S4$, $S5$, and $S6$ at $z = 0$, near the critical Rayleigh. These figures not only show that there is good agreement between the present stability analysis and the finite differences calculations carried out by Pallarès et al. (1999a), but also demonstrate that linear stability analysis is sufficient to describe qualitatively the type of flow structure developed near the critical Rayleigh. Of course, the differences become larger if the actual Ra goes away from the critical value at which the solution is born. Pallarès et al. (1999a) also reported a third

x or y–roll structure, $S3$, which seems to coincide with $S1$ at $Ra = 3500$, but presents different heat transfer characteristics at higher Ra.

Figures 10 and 11 show the vertical velocity and temperature fields at $z = 0$ of the stable structures $S1$ and $S5$ respectively for $Ra = 10^4$. Again there is good agreement between the non-linear stability analysis and the finite differences calculations.

In order to evaluate quantitatively the agreement between direct numerical simulation and the stability analysis shown in Figures 5 to 11, the numerical results were projected onto the corresponding subspace generated by the basis functions. This projection was carried out using the least-squares method and taking 250 trial functions, 125 in each of the two blocks associated to the structure, except for the diagonal roll structure $S2$ shown in Figure 6. In the case of $S2$ 75 trial functions of each block were taken because this structure involves trial functions from the four blocks M_1, M_4, M_6 and M_7. The choice was made according to the relevance of the eigenvalue.

The components of the projections together with the components predicted by stability analysis are depicted in Figures 12 to 13. It can be observed that there is good agreement, specially for the stable structure $S1$. The errors of the projections calculated as the square root of the sum of the squares of the differences between the numerical coefficients and those predicted by stability analysis are listed in Table III. The small values of the errors listed for $S1$, $S2$, $S4$ and $S5$ corroborate this agreement. Note also that part of the differences can be explained by the difficulties in the verification that a solution obtained by direct numerical simulation is close enough to a stationary one. In Figure 13, not so close to the Ra_c where the solutions originate, the agreement is excellent. Looking to Table III one checks, however, that the residues are similar to the other cases. This can be explained by the fact that, far from the critical Ra, there is a larger contribution of other modes.

7.2 Cavities with other aspect ratios

The present work is completed with the linear study of the dependence of the bifurcation Rayleigh numbers upon the aspects ratios depth/heigth and width/heigth (h_2, h_1) for parallelepipedic cavities. Considering the fact that $Ra_c(h_1, h_2) = Ra_c(h_2, h_1)$ the coordinates x and y can be exchanged and, thus, the bifurcation Rayleigh numbers can be estimated as a function of either h_2 or h_1, fixing either h_1 or h_2, respectively. Figure 14 shows the variation of the bifurcation Rayleigh number with h_2 for $h_1 = 0.5$, 1 and 2 over the range $0.5 \leq h_2 \leq 4.5$. The curves obtained by choosing the lowest bifurcation Rayleigh number present kinks at several values of h_2, as reported by Davis (1967), indicating transitions between the different possible structures.

The type of flow developed along any of the bifurcation curves shown in Figure 14 can be determined studying how the main modes of the associated normalized eigenvectors change continuously as a function of h_2. Figures 15 to 17 show the variation of the main modes of the eigenvectors as a function of h_2 along the different bifurcation curves plotted in Figure 14 for $h_1 = 1$. These computations were performed for $n_x = n_y = n_z = 5$ and rescaling the velocity field with respect to $Ra^{\frac{1}{2}}\,\vec{V}$, which is equivalent to normalise velocities with respect to κ/L. The numbers written below each curve indicate the number of the mode. The relationship between the number of mode, that of the block and the kind of roll developed (see Table I), together with the variation of the modes in Figures 15 to 17, allow the description of the transition along any bifurcation curve shown in Figure 14 for $h_1 = 1$.

From the variation of the principal velocity mode, i.e., the velocity mode with largest

absolute value, of the eigenvector of block M_1 with h_2, shown in Figure 15-a1, it can be observed that the type of flow developed along the bifurcation curve associated to this block corresponds with one x–roll (mode 1) for $0.5 \leq h_2 \leq 4.5$. The variation of the principal velocity modes associated with the block M_2, plotted in Figure 15-b1, indicates a transition from one y–roll with one change in the sense of rotation along its axis (mode 126) to one x–roll also with one change in the sense of rotation (mode 1). During this transition a structure, which is the sum of one x–roll and one y–roll, occurs when the two curves (modes 1 and 126) intersect in Figure 15-b1 at $h_2 = 1$. Thus, this intersection corresponds to the cubical geometry ($h_1 = h_2 = 1$).

Figure 16-a1 shows that the type of flow that takes place along the bifurcation curve associated to the block M_4 is an odd number of y–rolls. However, the number of y–rolls changes along the curve from one y–roll (mode 126) to three y–rolls (mode 131) and to five y–rolls (mode 136). The change in the number of y–rolls with h_2 occurs very rapidly, approximately where the bifurcation curve presents a maximum.

A similar behaviour can be observed in Figure 17-a1 for the modes corresponding to the first bifurcation Rayleigh number of block M_3 shown in Figure 14. In this case, however, the number of y–rolls involved is an even number. The main difference between blocks M_4 and M_3 is that the first transition for block M_3 takes place from a two x–rolls structure (mode 1) to a two y–rolls structure (mode 126), passing through a structure which is the sum of two x–rolls and two y–rolls (cubical case). Subsequent transitions in Figure 17-a1 are between an even number of rolls, beginning with a change from two y–rolls (mode 126) to four y–rolls (mode 131). The change in the number of y–rolls occurs again whenever the bifurcation curve presents a maximum. These transitions associated with blocks M_4 and M_3 differ from those reported by Davis (1967). He described a different curve for each k–number of y–rolls which would contradict the continuous (and even analytic) variation of the eigenvector with respect to the parameter h_2 shown in Figures 15 to 17.

Finally a comparison of critical Rayleigh numbers reported by Catton (1972) with those obtained in the present study and with the experimental data presented by Edwards and Sun (1970) is shown in Figure 18 for different values of h_2. There is good agreement between present results and literature data. It should be noted that experimental devices can not guarantee perfectly insulated lateral walls, a perfect geometry and vertical alignment of the experimental cavity, as discussed by Pallarès et al. (1999a).

8 Conclusions

The linear and non-linear stability analysis of the Rayleigh-Bénard flow inside a cubical cavity heated from below can be treated as an eigenvalue problem. The solutions of the perturbation equations for velocity and temperature, obtained with a Galerkin method by completing the set of trial functions proposed by Catton (1972), identify four critical Rayleigh numbers Ra = 3389, 5902, 7458 and 8610. At the first transition from the conductive state a x–roll and a diagonal-roll (x–roll $\pm$ y–roll) are formed. While the former is stable over the whole range of Ra studied ($Ra < 3 \times 10^4$) the latter is slightly unstable, with instability increasing with Rayleigh number. The single roll structure was identified numerically and experimentally by Pallarès et al. (1999a, b) over a wide range of Rayleigh numbers while the diagonal roll was also observed near the critical value. This discrepancy in the stability of the diagonal roll may be attributable to the stabilization caused by numerical diffusion in the finite volume calculations and by deviations in the adiabatic conditions at the four lateral walls, particularly near the vertical edges, in the

experiments.

The second bifurcation at $Ra = 5902$ yields a four rolls structure (x–roll + y–roll with both rolls changing sense of rotation at the two central orthogonal vertical planes). This initially unstable four rolls structure stabilizes beyond $Ra = 8900$, in agreement with previous numerical and experimental results. At $Ra = 7458$ a highly unstable $2x$–rolls + $2y$–rolls structure is formed while a $2x$–rolls − $2y$–rolls develops at $Ra = 8610$. The structure that develops at the last bifurcation is also unstable but with one of the dominant eigenvalues showing a tendency to change sign at higher Rayleigh numbers. Both structures were also identified numerically by Pallarès et al. (1999a) but were destabilized by small perturbations caused by changes in geometry and tilting of the cavity. The linear stability analysis of the effect of changing the aspect ratios of the cubical cavity on the bifurcation Rayleigh numbers shows that there is a continuous evolution of the flow towards multiple single roll configurations as the cavity elongates, with the axis of rotation parallel to the shortest side. These results are in agreement with other incomplete linear stability studies reported in the literature.

Acknowledgements The first and two last authors acknowledge the financial support received from DGICYT project no. PB93-0656-c0201 and PB96-1011. The second author has been partially supported by the Spanish grant DGICYT PB94-0215 and the Catalan grant CIRIT 1998SGR-42.

References

M. P. Arroyo, J.M. Saviron 1991 *Rayleigh-Bénard convection in a small box: spatial features and thermal dependence of the velocity field.* J. Fluid Mech., 235, 325–348.

F. H. Busse 1978 *Non-linear properties of thermal convection.* Rep. Prog. Phys., 41, 1929–1967.

F. H. Busse, R. M. Clever 1979 *Instabilities of convection rolls in a fluid of moderate Prandtl number.* J. Fluid Mech., 91, 319–335.

F. H. Busse 1981 *Transition to turbulence in Rayleigh-Bénard convection.* In H. L. Swinney, J. P. Gollub, editors, *Hydrodynamic instabilities and the transition to turbulence*, 97–137, Springer, New York.

C. Canuto, M.Y. Hussaini, A. Quarteroni, T.A. Zang 1987 *Spectral Methods in Fluid Dynamics.* Springer Series in Computational Physics. Springer Verlag. New York.

I. Catton 1971 *The effect of insulating vertical walls on the onset of motion in a fluid heated from below.* Int. J. Heat Mass Transfer, 5, 665–672.

S.H. Davis 1967 *Convection in a box: linear theory.* J. Fluid Mech., 30, 465–478.

D.K. Edwards, W.M. Sun 1970 *Predictions of the onset of natural convection in rectangular honeycomb structures.* Int. Solar Energy Society Conference, Melbourne (2-6 March 1970).

D.L. Harris, W.H. Reid 1959 *On orthogonal functions which satisfy four boundary conditions.* Astrophys. J. Suppl. Ser.,3, 429–452.

W.L. Heitz, J.W. Westwater 1971 *Critical Rayleigh numbers for natural convection of*

water confined in square cells with L/D from 0.5 *to* 8 ASME J. Heat Transfer, 93, 188–196.

R. Hernández, R.L. Frederick 1994 *Spatial and thermal features of three dimensional Rayleigh-Bénard convection.* Int. J. Heat Mass Transfer, 37, 411–424.

E.L. Koschmieder 1993 *Bénard Cells and Taylor Vortices* Cambridge Monographs on Mechanics and Applies Mathematics. Cambridge University Press. Cambridge.

D. Mukutmoni and K.T. Yang 1994 *Flow transitions and pattern selection of the Rayleigh-Bénard problem in rectangular enclosures* Sadhana, 19, 649–670.

C. Normand, Y. Pomeau and M. G. Velarde 1977 *Convective instability: A physicist's approach* Rev. of Modern Phys., 49, 581–624.

H. Oertel 1982 *Thermal instabilities.* In J. Zierep and H. Oertel, editors, *Convective Transport and Instability Phenomena*, 3–24, Karlsruhe.

J. Pallarès, F.X. Grau, F. Giralt 1999a *Flow transitions in laminar Rayleigh-Bénard convection in a cubical cavity at moderate Rayleigh numbers.* Int. J. Heat Mass Transfer, 42, 753–769.

J. Pallarès, M.P. Arroyo, F.X. Grau and F. Giralt 1999b *Experimental laminar Rayleigh-Bénard convection in a cubical cavity at moderate Rayleigh and Prandtl numbers.* Submitted to Experiments in Fluids.

M. Sherman, S. Ostrach 1966 *On the principle of exchange of stabilities for the magneto-hydrodynamic thermal stability problem in completely confined fluids.* J. Fluid Mechanics, 24, 661–671.

R.E. Showalter 1979 *Hilbert Space Methods for Partial Differential Equations.* Pitman Advanced Publishing Program. Pitman Press. Bath.

C. Simó 1990 *Analytical and numerical computation of invariant manifolds.* In D. Benest et C. Froeschlé, editors, *Modern methods in celestial mechanics*, 285–330, Editions Frontières, Paris.

K. Stork, U. Müller 1972 *Convection in boxes: experiments.* J. Fluid Mech., 54, 599–611.

K.T. Yang 1988 *Transitions and bifurcations in laminar buoyant flows in confined enclosures.* ASME J. Heat Transfer, 110, 1191–1204.

Table I: Examples of the kind of roll that developes for $n_x = n_y = n_z = 5$. The fourth and the fifth column indicate the number of changes in the sense of rotation that occur around x or y axis and the z coordinate, respectively.

Function number	**Block number**	**Kind of roll**	**Changes along the roll axis**	**Changes along z**
1	1	one x–roll	0	0
1	2	one x–roll	1	0
1	3	two x–rolls	0	0
126	2	one y–roll	1	0
126	3	two y–rolls	0	0
126	4	one y–roll	0	0
131	3	four y–rolls	0	0
131	4	three y–rolls	0	0

Table II: Critical Rayleigh numbers and type of flow structure developed at the bifurcations from the conductive state in a cubical geometry.

Type of structure	**Catton** (1972)	**Hernández** (1994)	**Pallarès et al.** (1999a)	**Present work**
x–roll ($S1$)	3446	–	3500	3389
diagonal–roll ($S2$)	–	–	3500	3389
four rolls ($S5$)	–	–	6000	5902
$2x$–rolls + $2y$–rolls ($S4$)	–	8000	7800	7458
$2x$–rolls − $2y$–rolls ($S6$)	–	–	–	8610

Table III: Error of the projections between the direct numerical simulations and stability analysis results.

Structure	**Ra**	**Error**
$S1$	3500	0.5270×10^{-2}
$S2$	3500	0.9121×10^{-2}
$S5$	6500	0.4138×10^{-2}
$S4$	7800	0.8823×10^{-2}
$S1$	10000	0.6887×10^{-2}
$S5$	10000	0.9700×10^{-2}

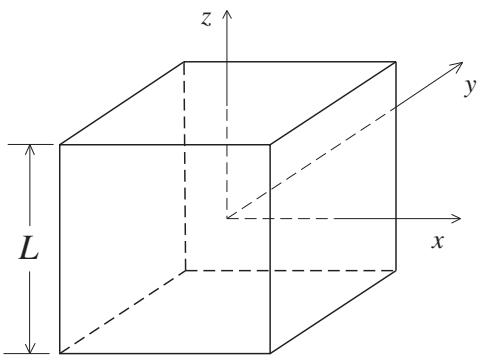

Figure 1: Coordinate system of the cubical region Ω

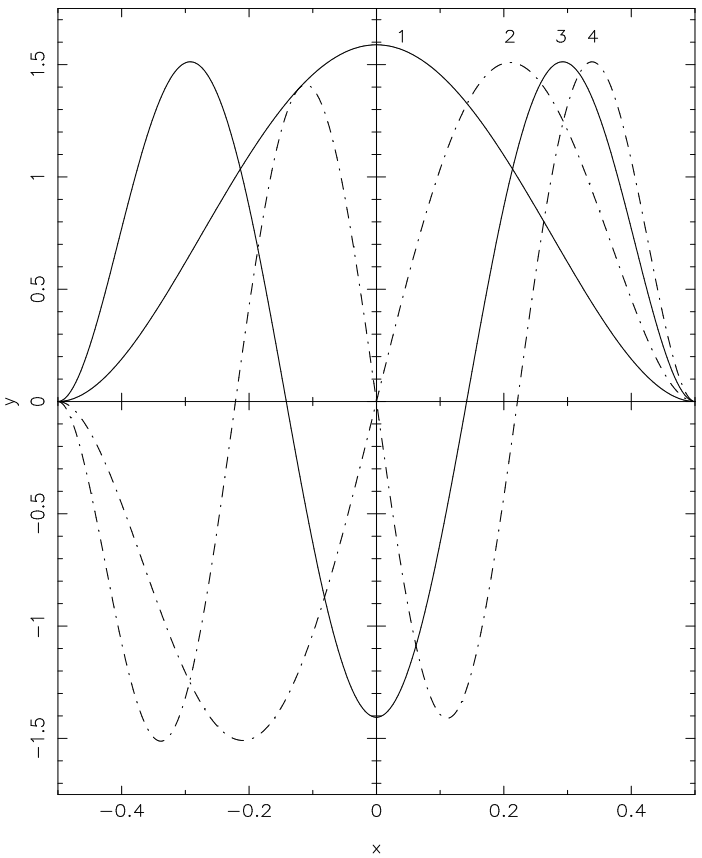

Figure 2: The curves marked 1,2,3,4 represent $C_1(x)$, $S_1(x)$, $C_2(x)$, and $S_2(x)$, respectively.

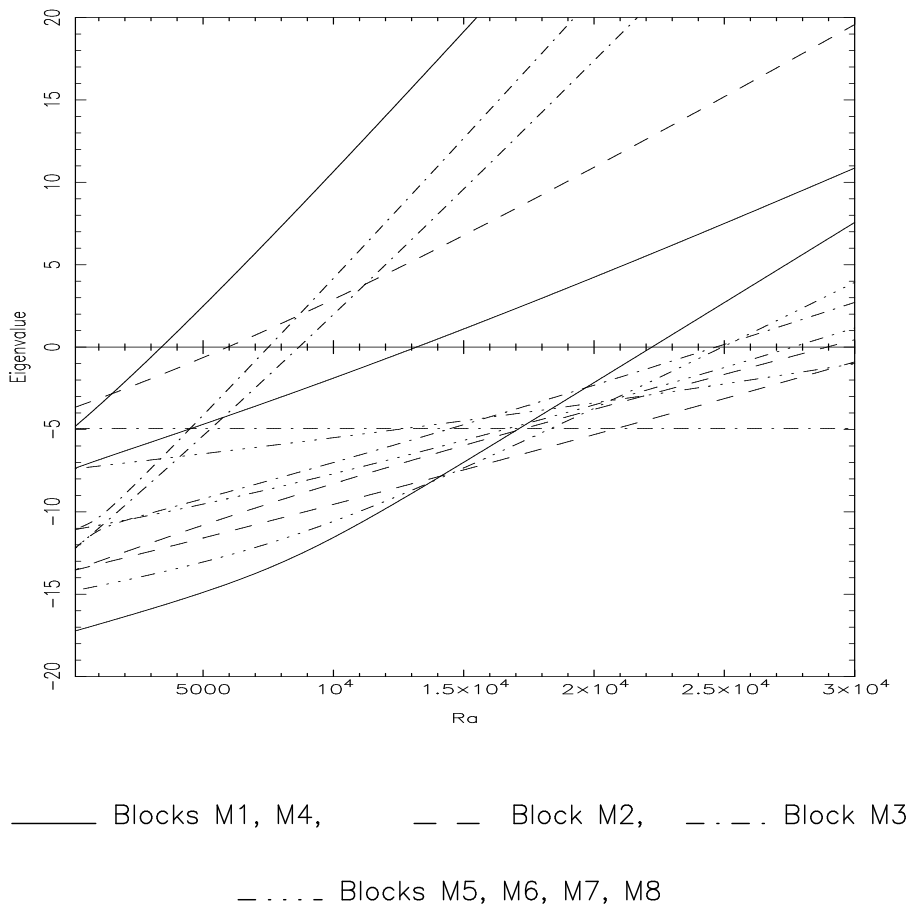

Figure 3: Several of the largest eigenvalues of M_i $1 \leq i \leq 8$ as a function of Ra for the cubical cavity.

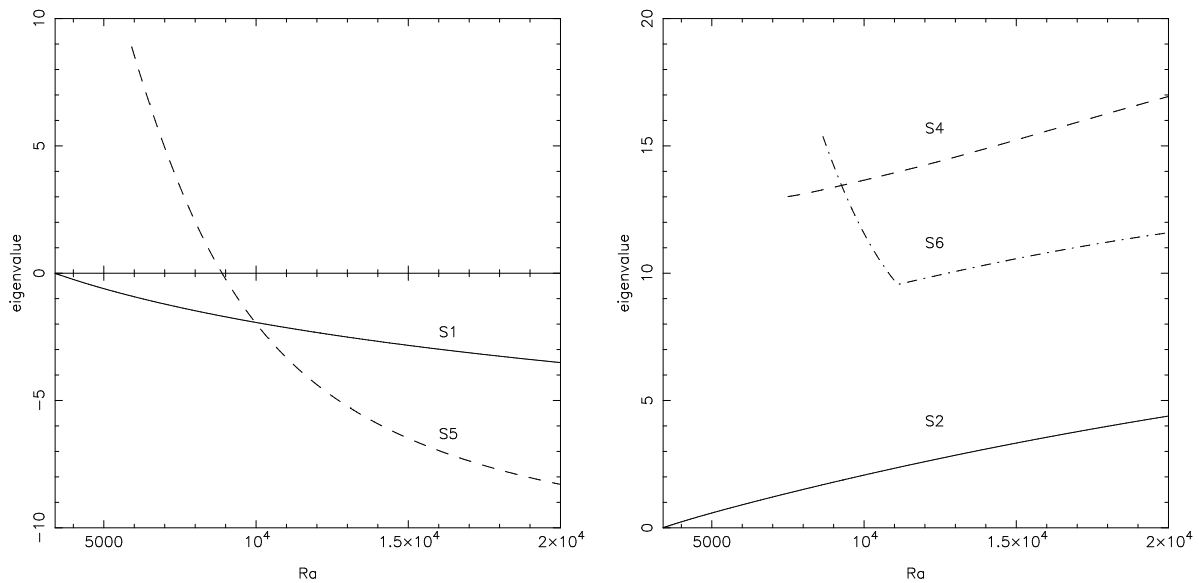

a) Stable structures $S1$ and $S5$ b) Unstable structures $S2$, $S4$ and $S6$

Figure 4: Variation of the principal eigenvalue as a function of Ra.

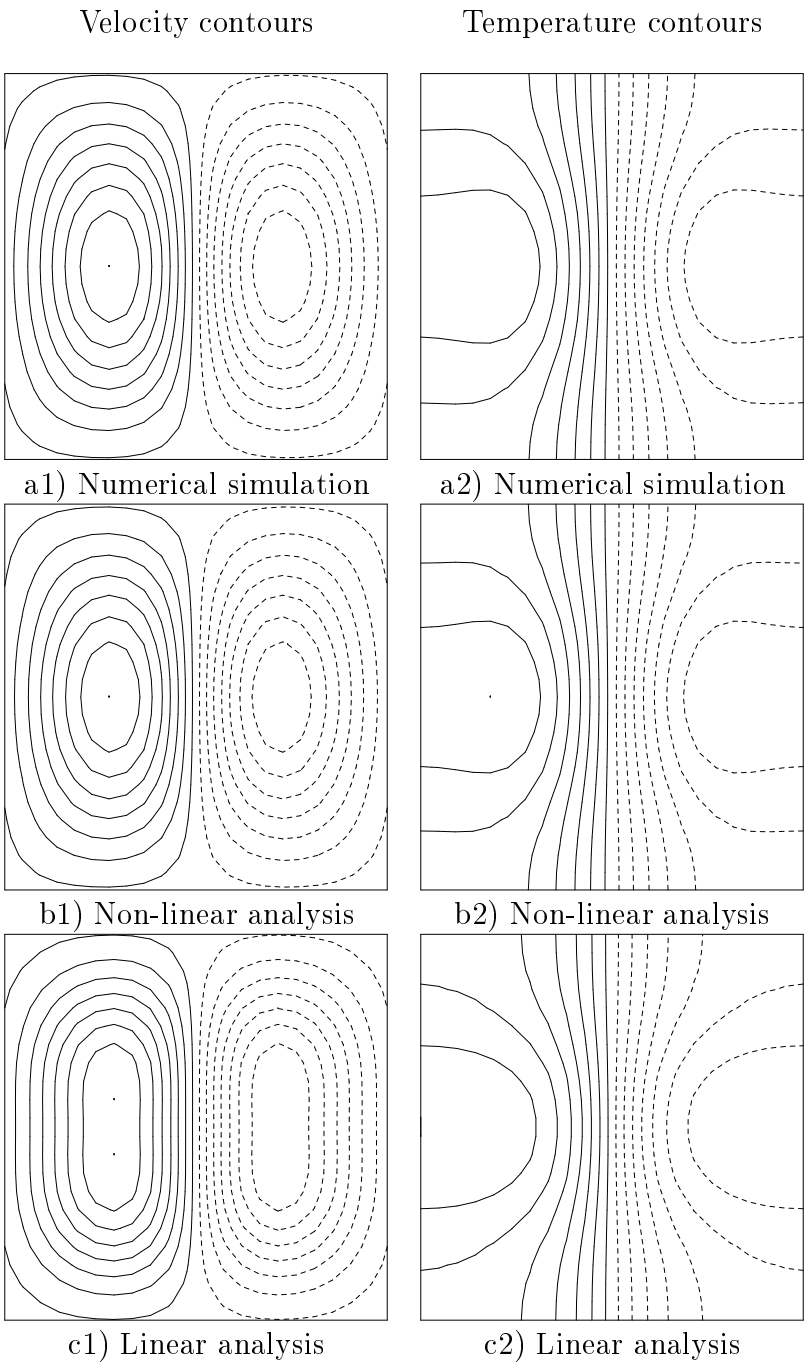

Figure 5: Vertical velocity contours and temperature contours in the horizontal midplane $z = 0$ for the one x–roll stable structure $S1$ Figures (a1-a2) and (b1-b2) show the contours obtained by numerical simulation by Pallarès et al. and the contours predicted by non-linear stability analysis at $Ra = 3500$. The contours predicted by linear stability analysis at the critical $Ra = 3389$ are depicted in figures (c1-c2). Continuous and discontinuous lines refer to positive and negative values, respectively. The same convention has been used in the next Figures.

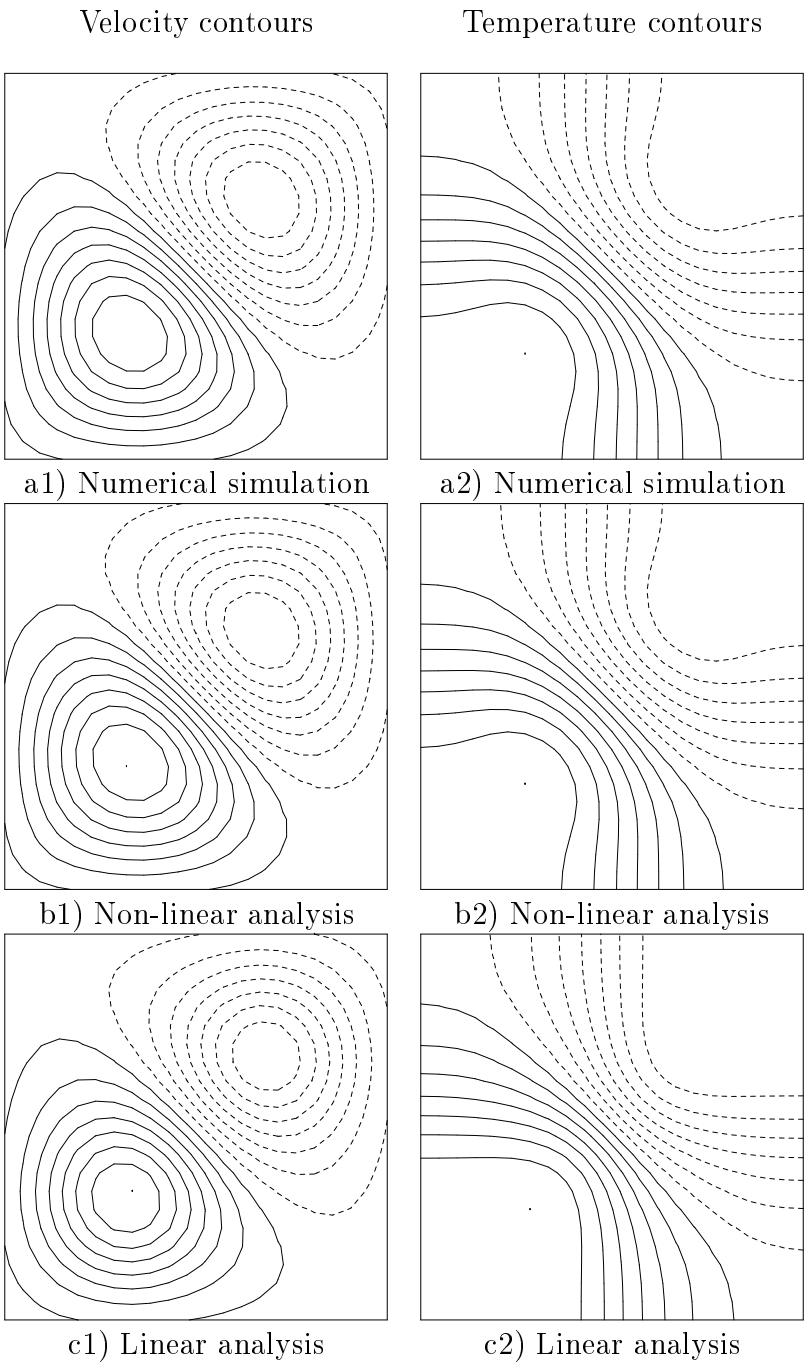

Figure 6: Vertical velocity contours and temperature contours in the horizontal midplane $z = 0$ for the one diagonal roll unstable structure $S2$ Figures (a1-a2) and (b1-b2) show the contours obtained by numerical simulation by Pallarès et al. and the contours predicted by non-linear stability analysis at $Ra = 3500$. The contours predicted by linear stability analysis at the critical $Ra = 3389$ are depicted in figures (c1-c2).

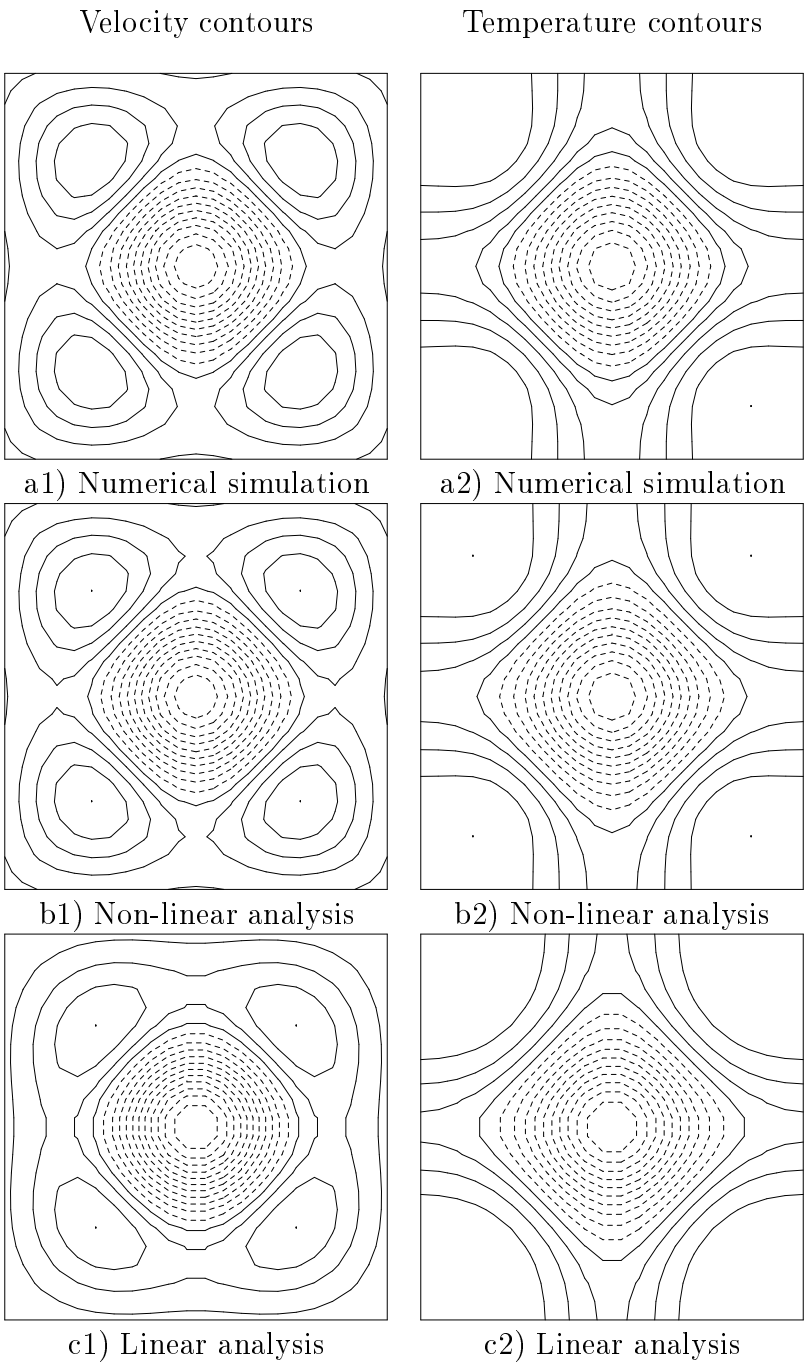

Figure 7: Vertical velocity contours and temperature contours in the horizontal midplane $z = 0$ for the structure unstable $S4$. Figures (a1-a2) and (b1-b2) show the contours obtained by numerical simulation by Pallarès et al. and the contours predicted by non-linear stability analysis at $Ra = 7800$. The contours predicted by linear stability analysis at the critical $Ra = 7458$ are depicted in figures (c1-c2).

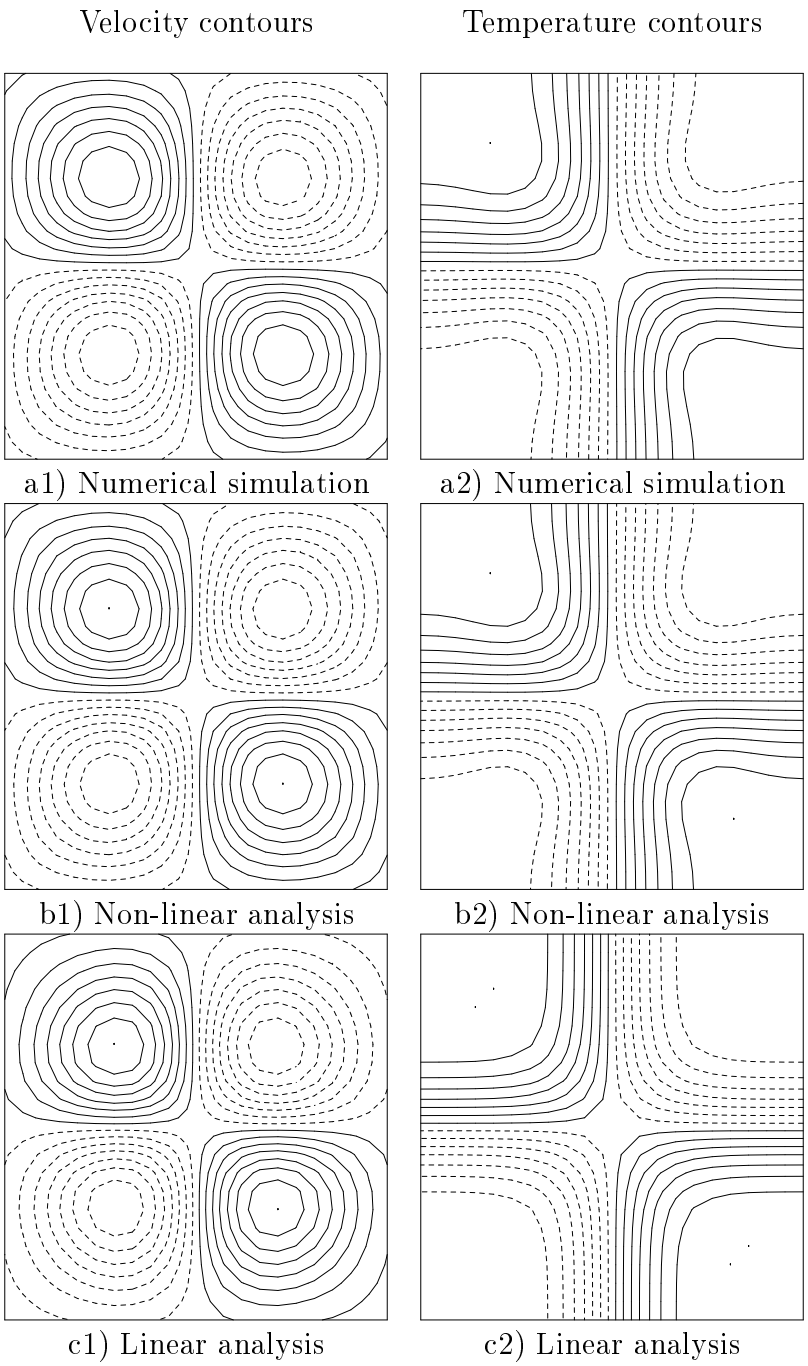

Figure 8: Vertical velocity contours and temperature contours in the horizontal midplane $z = 0$ for the structure $S5$. Figures (a1-a2) and (b1-b2) show the contours obtained by numerical simulation by Pallarès et al. and the contours predicted by non-linear stability analysis at $Ra = 6500$. The contours predicted by linear stability analysis at the critical $Ra = 5902$ are depicted in figures (c1-c2).

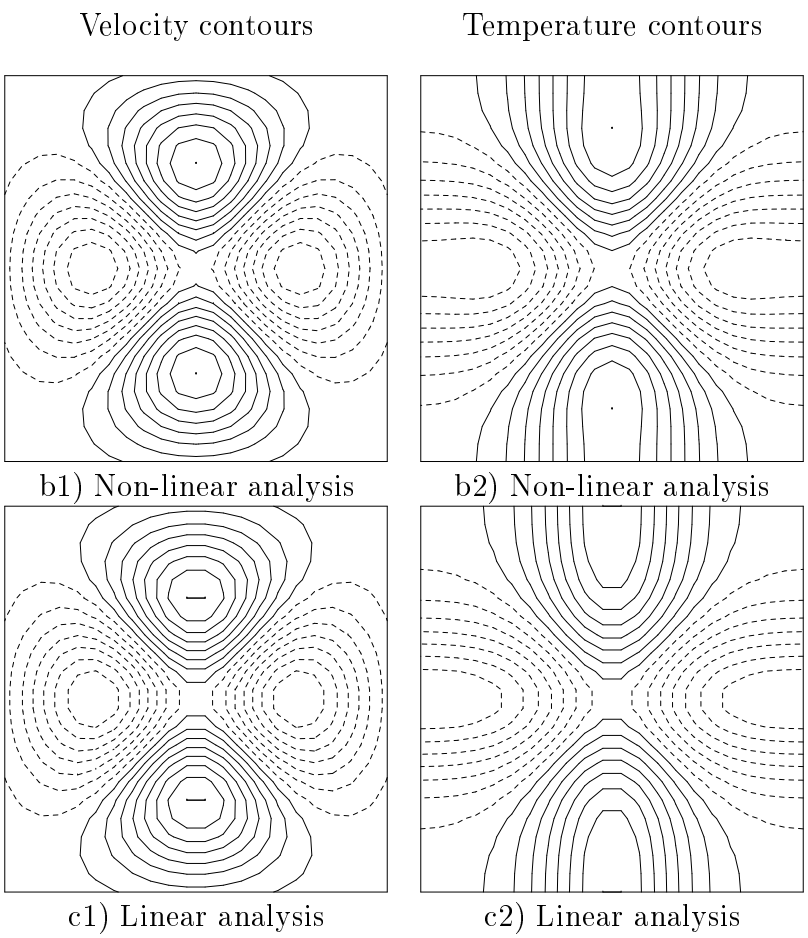

Figure 9: Vertical velocity contours and temperature contours in the horizontal midplane $z = 0$ for the structure $S6$. Figures (b1-b2) show the contours predicted by non-linear stability analysis at $Ra = 9500$. The contours predicted by linear stability analysis at the critical $Ra = 8610$ are depicted in figures (c1-c2).

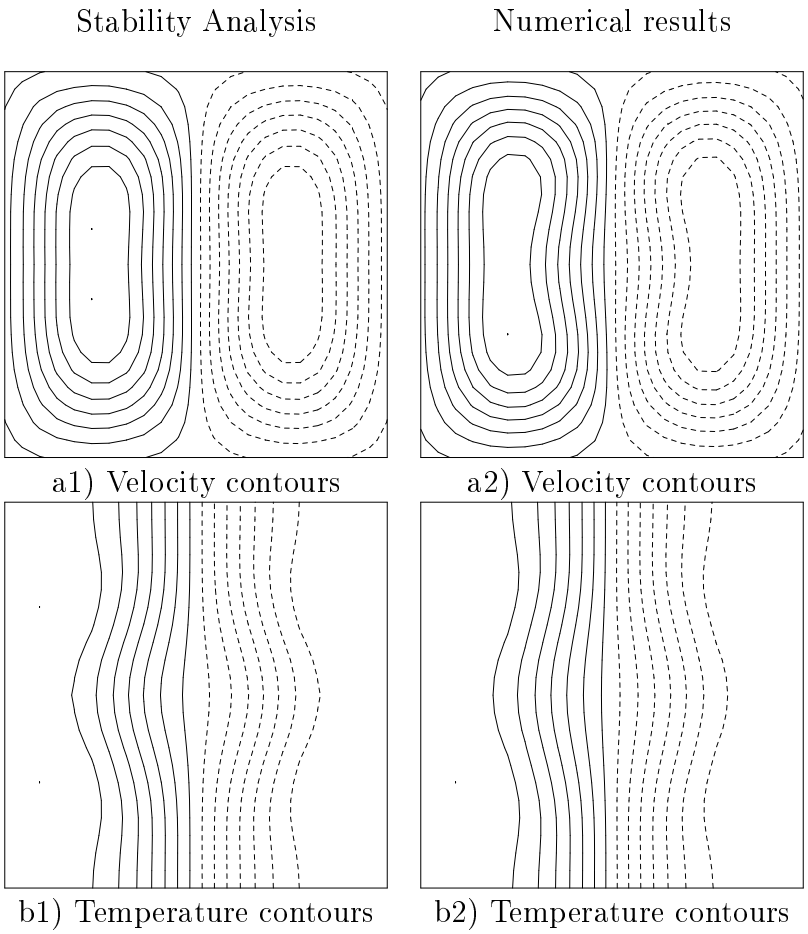

Figure 10: Vertical velocity contours and temperature contours in the horizontal midplane $z = 0$ for the stable structure $S1$ at $Ra = 10^4$. Figures (a1, b1) show the contours predicted by stability analysis and the contours obtained by numerical simulation by Pallarès et al. are depicted in figures (a2, b2).

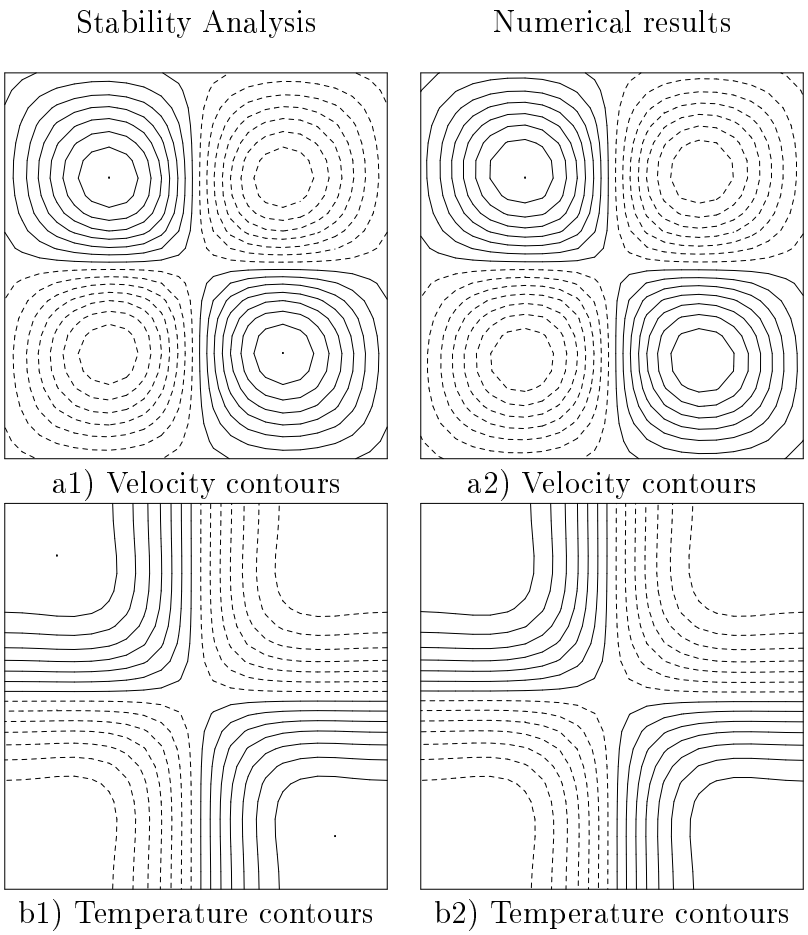

Figure 11: Vertical velocity and temperature contours in the horizontal midplane $z = 0$ for the structure $S5$ at $Ra = 10^4$. Figures (a1, b1) show the contours predicted by stability analysis. The contours obtained by numerical simulation are depicted on figures (a2, b2).

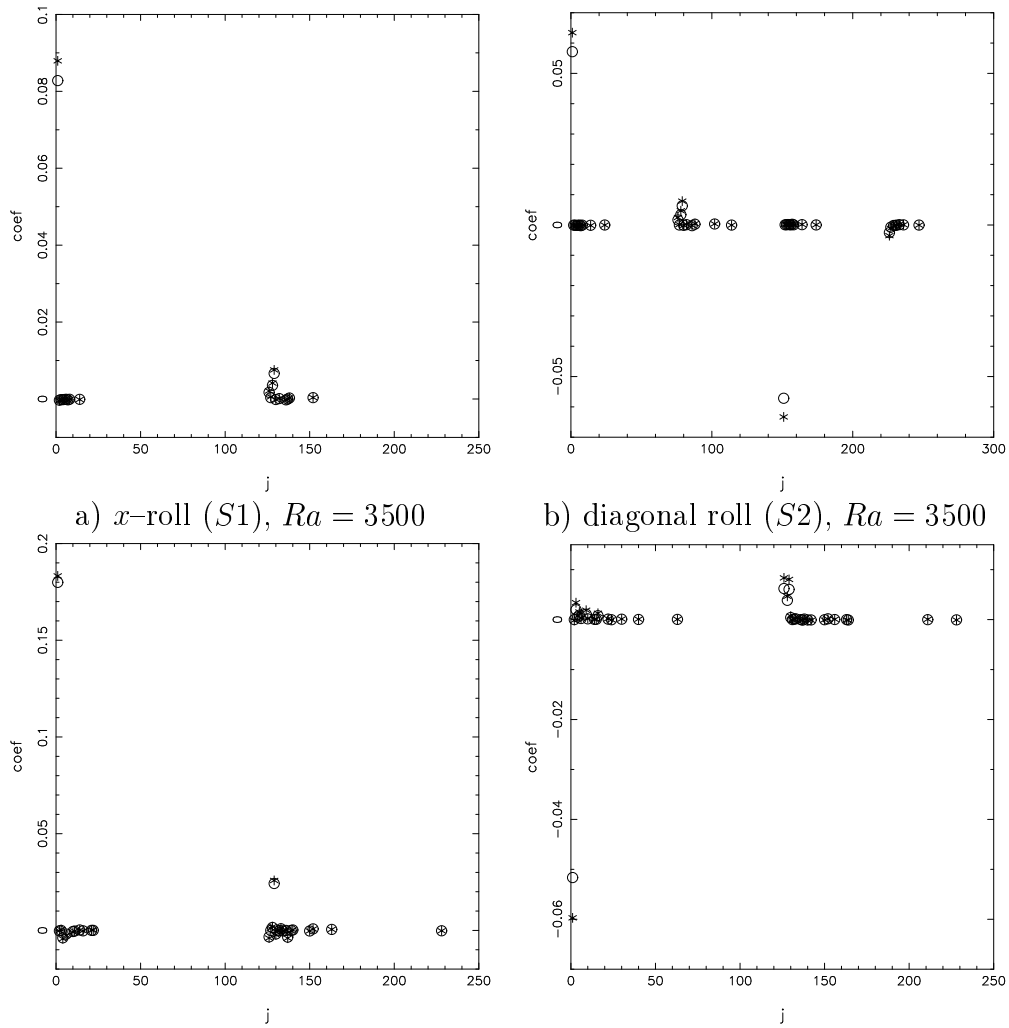

a) x–roll ($S1$), $Ra = 3500$ b) diagonal roll ($S2$), $Ra = 3500$

c) x–roll + y–roll ($S5$), $Ra = 6500$ d) $2x$–roll+$2y$–roll ($S4$), $Ra = 7800$

$*$ Numerical Results. $\circ$ Stability Analysis predictions.

Figure 12: Components of the projections of the flows predicted numerically onto the subspace generated by the trial functions near the different bifurcation Rayleigh numbers. The index j indicates the number of the component. Only components larger than 10^{-3} times the greatest component have been retained.

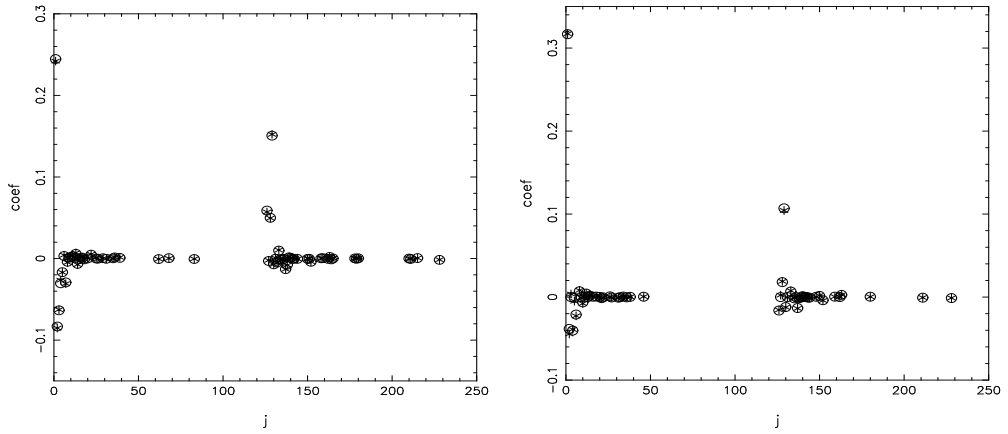

a) x–roll structure ($S1$) b) x–roll + y–roll structure ($S5$)

$*$ Numerical Results. $\circ$ Stability Analysis predictions.

Figure 13: Components of the projections of the stable flows predicted numerically onto the subspace generated by the trial functions at $Ra = 10000$. The index j indicates the number of the component. Only components larger than 10^{-3} times the greatest component have been retained.

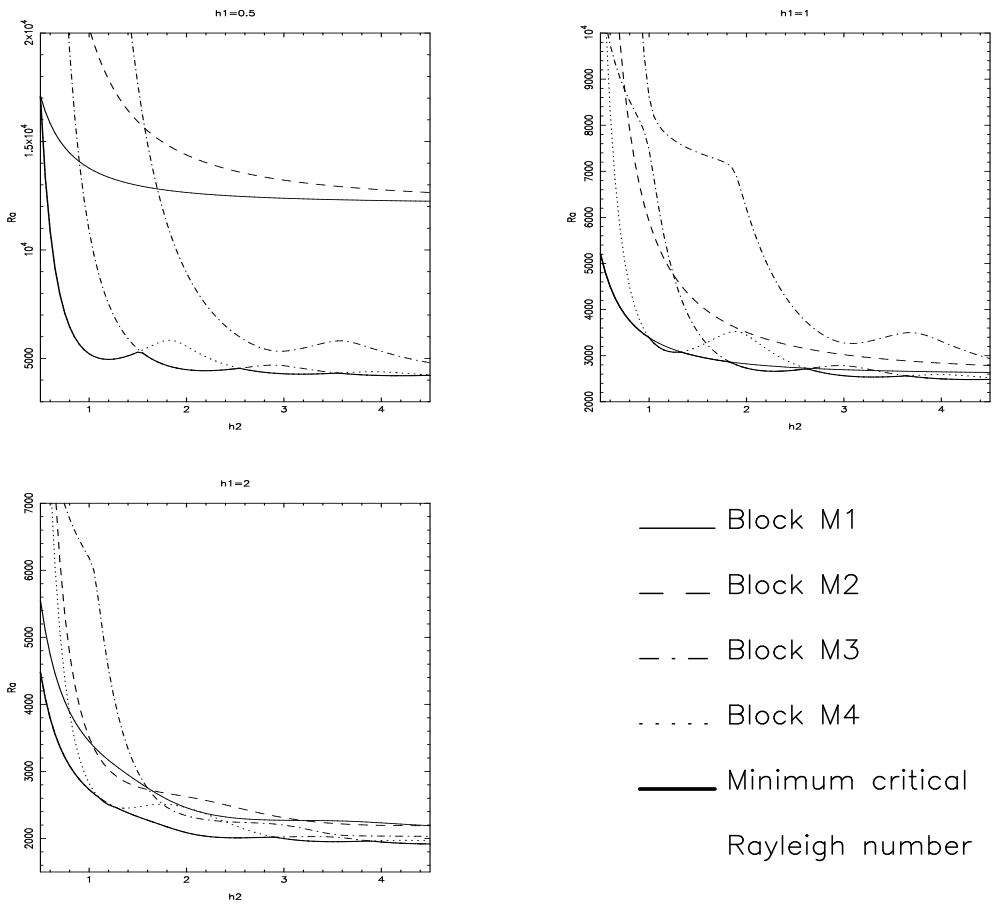

Figure 14: Bifurcation Rayleigh numbers as a function of the aspect ratio h_2 for $h_1 = 0.5$, 1 and 2. For $h = 0.5$ and $h = 2$, the critical value is associated to blocs M_3 or M_4. In the case $h = 1$, also M_1 appears.

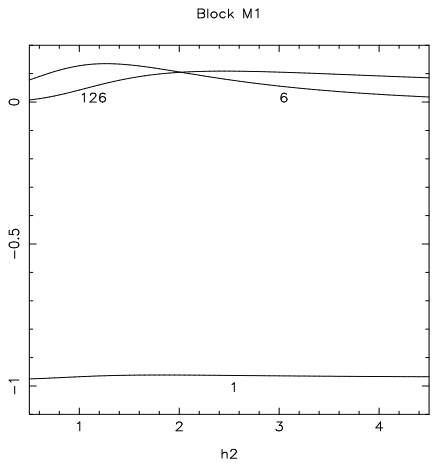

a1)velocity modes

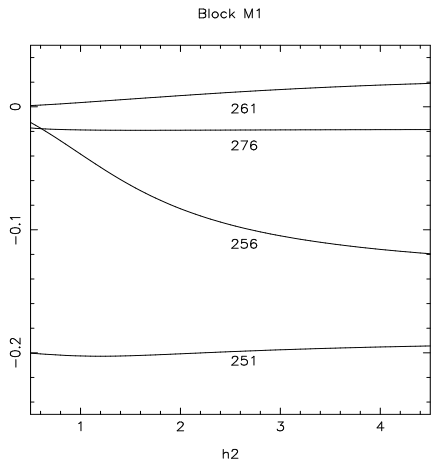

a2) temperature modes

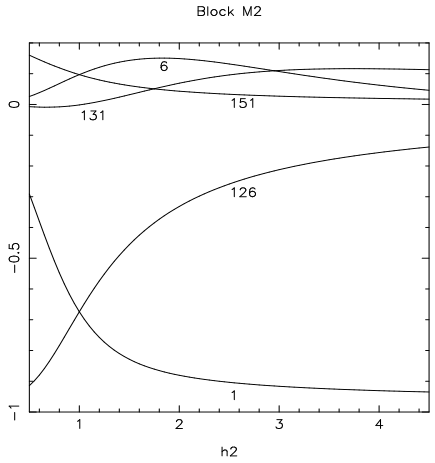

b1)velocity modes

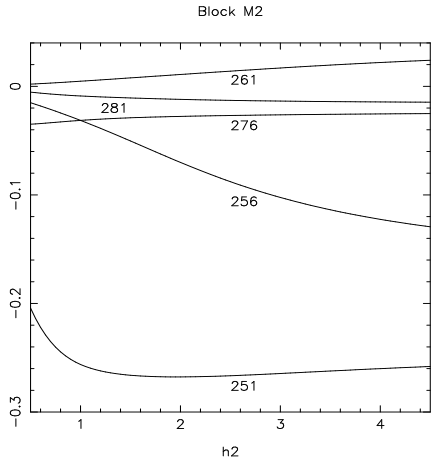

b2) temperature modes

Figure 15: Variation of principal modes of the eigenvectors as a function of h_2 along the bifurcation curves associated to the blocks M_1 and M_2 for $h_1 = 1$ and $0.5 \leq h_2 \leq 4.5$.

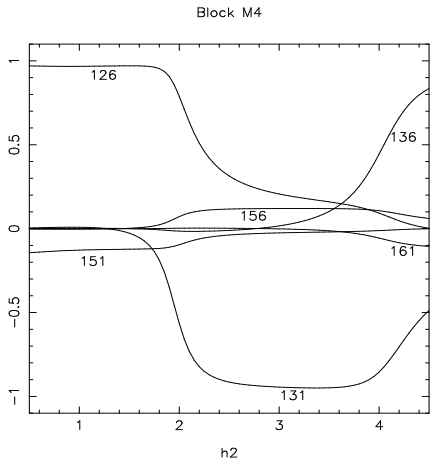

a1)velocity modes

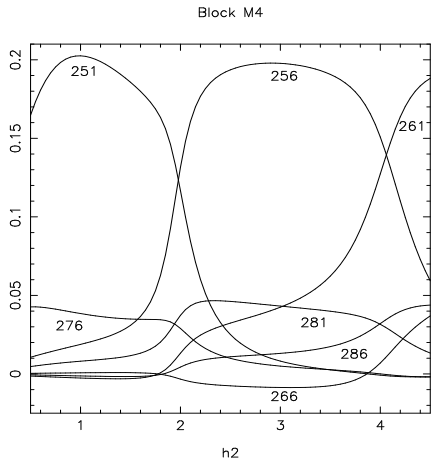

a2) temperature modes

Figure 16: Variation of principal modes of the eigenvectors as a function of h_2 along the bifurcation curve associated to the block M_4 for $h_1 = 1$ and $0.5 \leq h_2 \leq 4.5$.

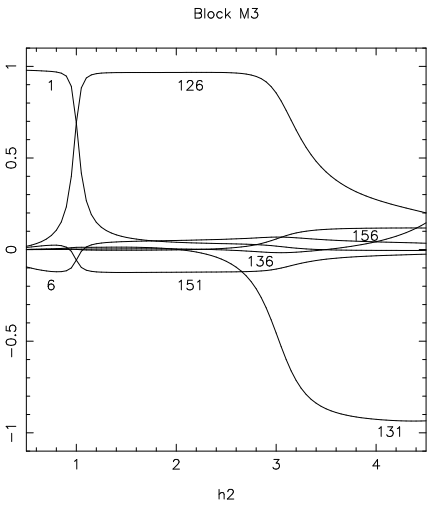

a1)velocity modes

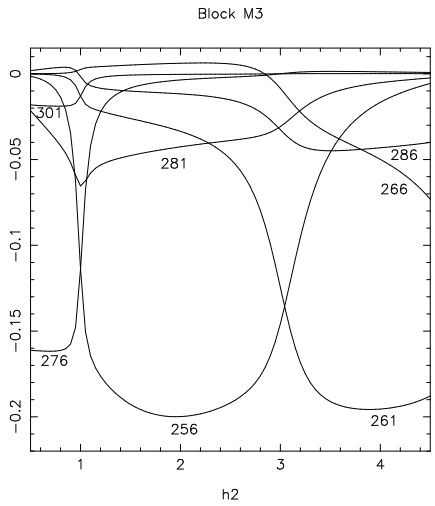

a2) temperature modes

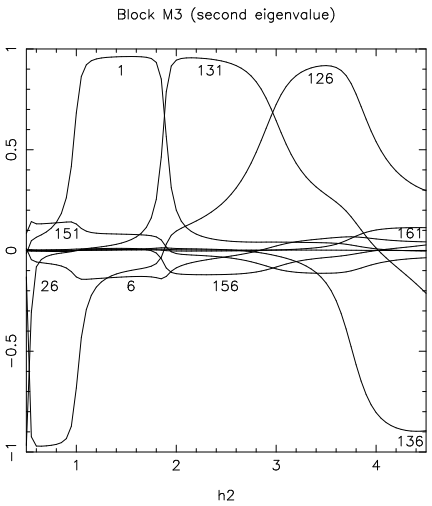

b1)velocity modes

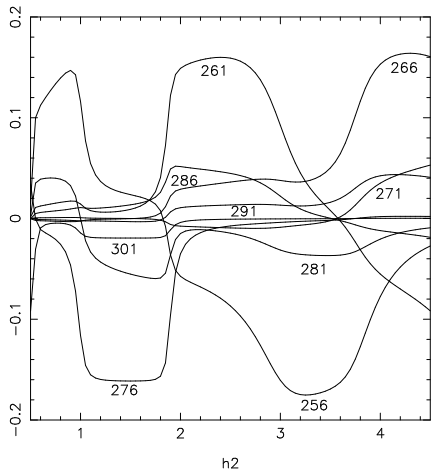

b2) temperature modes

Figure 17: Variation of principal modes of the eigenvectors as a function of h_2 along the bifurcation curves associated to the block M_3 for $h_1 = 1$ and $0.5 \leq h_2 \leq 4.5$.

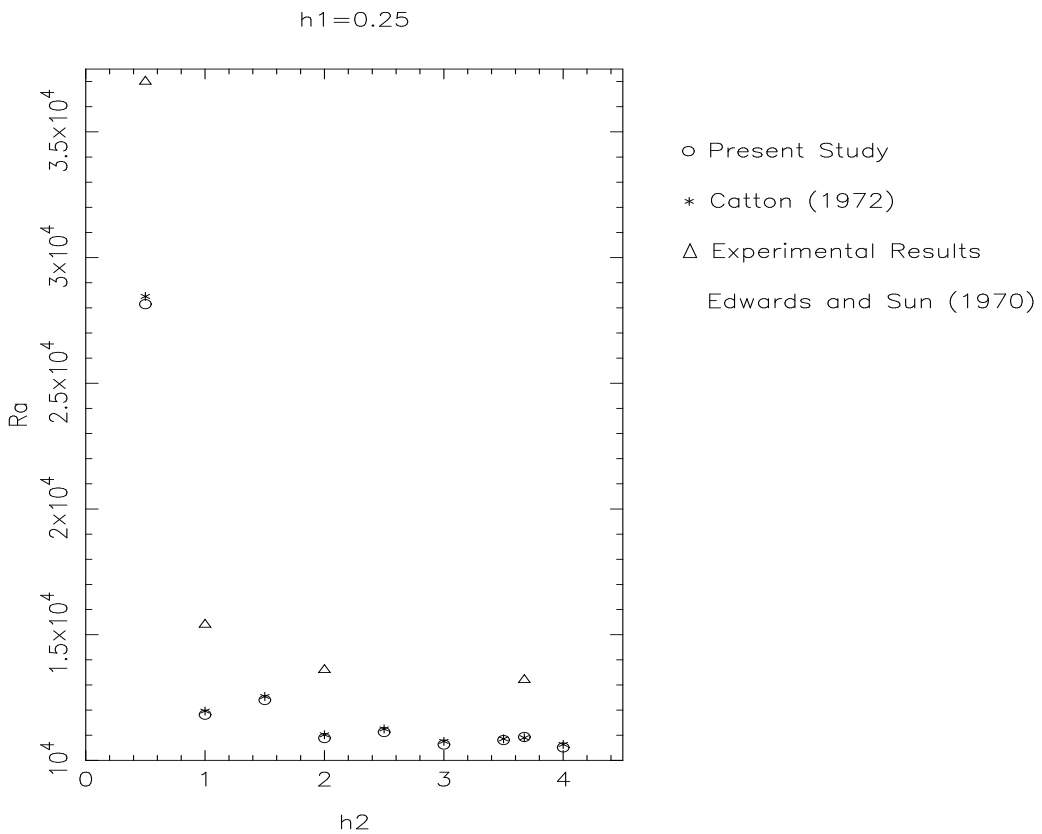

Figure 18: Comparison of critical Rayleigh numbers reported by Catton with those obtained in the present study and with the experimental data reported by Edwards and Sun (1990) for different values of h_2.